Research Square

Preprints are preliminary reports that have not undergone peer review.
They should not be considered conclusive, used to inform clinical practice,
or referenced by the media as validated information.

Dielectric barrier discharge (DBD) plasma delays postharvest senescence of sweet corn via an AsA–GSH-mediated multi-pathway synergistic network

Jingjing Jin
Beijing Academy of Agriculture and Forestry Sciences
Ronghuan Wang
Beijing Academy of Agriculture and Forestry Sciences
Tianjun Xu
Beijing Academy of Agriculture and Forestry Sciences
Christopher B. Watkins
Beijing Academy of Agriculture and Forestry Sciences
Yunxiang Wang
Beijing Academy of Agriculture and Forestry Sciences
Yiting Ren
Beijing Academy of Agriculture and Forestry Sciences
Hua Chen
Beijing Academy of Agriculture and Forestry Sciences
Chunmei Bai
Beijing Academy of Agriculture and Forestry Sciences
Kunyu Sun
Beijing Academy of Agriculture and Forestry Sciences
Lili Ma
Beijing Academy of Agriculture and Forestry Sciences
Xuelian He
Beijing Academy of Agriculture and Forestry Sciences
Zhaorui Li
Beijing Academy of Agriculture and Forestry Sciences
Lihong Wang
Hebei University of Engineering
Jinhua Zuo
zuojinhua@126.com

Beijing Academy of Agriculture and Forestry Sciences
Yanyan Zheng

Beijing Academy of Agriculture and Forestry Sciences

Article

Keywords: Dielectric barrier discharge plasma, Antioxidant system, Reactive oxygen species, Senescence regulation, Plant hormone signaling

Posted Date: November 23rd, 2026

DOI: https://doi.org/10.21203/rs.3.rs-11436964/v1

License: This work is licensed under a Creative Commons Attribution 4.0 International License. Read Full License

Additional Declarations: No competing interests reported.

Dielectric barrier discharge (DBD) plasma delays postharvest senescence of sweet corn via an AsA–GSH-mediated multi-pathway synergistic network

Jingjing Jin[a, b, 1], Ronghuan Wang[c, 1], Tianjun Xu[c, 1], Christopher B. Watkins[a] Yunxiang Wang[a], Yiting Ren[a], Hua Chen[a], Chunmei Bai[a], Kunyu Sun[a], Lili Ma[a], Xuelian He[a], Zhaorui Li[a], Lihong Wang[b, *], Jinhua Zuo[a, *], Yanyan Zheng[a, *].

[a] Key Laboratory of Fruits and Vegetable Storage and Processing State, Key Laboratory of Vegetable Postharvest Processing, Ministry of Agriculture and Rural Affairs, Key Laboratory of Vegetable Biobreeding, Beijing Vegetable Research Center, Institute of Agro-Products Processing and Food Nutrition, Beijing Academy of Agriculture and Forestry Sciences, Beijing 100097, China.

[b] School of Life Sciences and Food Engineering, Hebei University of Engineering, Handan 056038, China.

[c] Institute of Maize. Beijing Academy of Agriculture and Forestry Sciences, Beijing 100097, China

Corresponding author: Yanyan Zheng (jxzhengyanyan@163.com); Jinhua Zuo (zuojinhua@126.com); Lihong Wang (18710354317@163.com)

1 These authors contributed equally to this work. (Email address: Jingjing Jin: 15903204340@163.com; Ronghuan Wang: ronghuanwang@126.com; Tianjun Xu: xtjxtjbb@163.com)

Abstract:

Harvested sweet corn (*Zea mays* L.) have high respiration rates and are susceptible to water-loss and shriveling, loss of sweetness and color as well as kernel hardening (increased firmness). The effects of dielectric barrier discharge (DBD) plasma (10.5 kV, 10 min) on the senescence of 'Nongkenuo 336' sweetcorn kept at 20 °C and 90% ± 2% relative humidity for up to 8 days were investigated. Physiological measurements were combined with transcriptomic, widely targeted metabolomic, and proteomic analyses to dissect the molecular mechanisms by which DBD plasma affects sweet corn metabolism. DBD treatment suppressed kernel hardening, weight loss, and loss of soluble solids content and color. 1196 differentially accumulated metabolites were identified and DBD treatment inhibited the progressive accumulation of deterioration-associated metabolites senescenceover time, while maintaining flavor- and nutrition-related metabolites. Transcriptomics showed that DBD treatment repressed starch-hydrolyzing genes (*AMY*, *BAM*), ethylene signaling genes (*ETR*, *EIN2*, *EIN3*), and the cell wall degradation gene, *PME*. DBD treatment maintained expression of phenylpropanoid pathway genes (*PAL*, *HCT*, *COMT*, *CAD*, *POD*), the ABA receptor, *PYL*, and the response factor, *ABF*, while downregulating the signal amplifier *SnRK2*. Proteomics revealed significant enrichment of defense-related proteins, including glutathione S-transferase family proteins and UDP-glucuronosyl/UDP-glucosyl transferase family proteins. Notably, ascorbate–glutathione (AsA–GSH) metabolism was enriched across all three omic measurement: *GlcAK* expression recovered, and antioxidant metabolites such as L-ascorbic acid were maintained. Together, these results indicate that DBD plasma activates an antioxidant network centered on the AsA–GSH cycle. This network coordinately regulates hormone

signaling, sugar metabolism, cell wall metabolism, and secondary metabolism, converting exogenous RONS-induced oxidative signals into protective physiological responses that are associated with the systematic delay of senescence.

Keywords: Dielectric barrier discharge plasma; Antioxidant system; Reactive oxygen species; Senescence regulation; Plant hormone signaling

Introduction

Sweet corn (*Zea mays* L.) combines the nutritional attributes of cereals and vegetables. It is rich in dietary fiber, vitamins, antioxidants, and other bioactive compounds (Mushtaq et al., 2025). Sweet corn is shifting from a seasonal crop to a year-round premium healthy food, and global demand continues to expand (Becerra-Sanchez and Taylor, 2021). As the China cultivates more than 530,000 hectares, ranking first globally in production (Xiao et al., 2024). However, sweet corn has high respiration rates after harvest, and quality deteriorates rapidly, with water-loss, shriveling, kernel hardening (increased firmness), loss of sweetness and flavor loss, and off-odor development, that constrain market expansion (Chen et al., 2024; Chen et al., 2026a). New postharvest preservation technologies are needed to reduce postharvest losses and extend the supply window for consumers.

The primary method to maintain quality of sweet corn is cold storage but is highly cold-chain dependent and sensitive to temperature fluctuations (Becerra-Sanchez and Taylor, 2021). In recent years, cold plasma has attracted wide attention as a novel non-thermal physical preservation technology (Nikzadfar et al., 2024). Dielectric barrier discharge (DBD) generates reactive oxygen and nitrogen species (RONS) at ambient temperature and pressure, including ozone (O_3), hydrogen peroxide (H_2O_2), hydroxyl

radicals (·OH), superoxide anions ($O_2 \cdot^-$), and nitric oxide (NO). These species can delay postharvest senescence and quality deterioration of fruit and vegetables through multiple mechanisms, such as inducing oxidative stress or activating antioxidant systems (Singh and Thakur, 2024). It is therefore one of the most promising plasma technologies for postharvest preservation of fruit and vegetables (Nikzadfar et al., 2024; Shishir et al., 2025). DBD can operate at ambient temperature and pressure, readily enabling in-package treatment, and it has relatively low equipment costs. Previous studies have demonstrated the efficacy of DBD treatment in in-package sterilization and preservation of strawberries and spinach (Ziuzina et al., 2020). It can also regulate color and phenolic metabolism in blueberries (Xu et al., 2024) and maintain chlorophyll metabolism in tomatoes (Jia et al., 2022). In addition, it maintains firmness and inhibits browning in button mushrooms (Subrahmanyam et al., 2023) and controls browning in fresh-cut apples (Tappi et al., 2019). However, no studies have yet reported the effects of DBD treatment on postharvest physiological metabolism and quality deterioration of sweet corn, and the underlying molecular mechanisms remain to be elucidated.

This study therefore focused on the application potential of DBD plasma in sweet corn preservation. Using optimized treatment parameters (10.5 kV, 10 min), we systematically evaluated its efficacy in maintaining postharvest storage quality. To elucidate the underlying molecular mechanisms, we analyzed its regulatory effects on postharvest physiological quality, energy metabolism, cell wall metabolism, and antioxidant systems. We did so from three dimensions: gene expression profiles, metabolite dynamics, and protein functional networks. This work systematically clarifies the molecular basis by

which DBD treatment delays quality deterioration and extends the storage period of sweet corn.

Results

Firmness, color, soluble solids content, and weight loss

DBD plasma treatment delayed postharvest quality deterioration of sweet corn. cobs Firmness as a measure of kernel hardening increased over time, but to a greater extent in the untreated (CK) than the DBD ones (Fig. 1A). The DBD treated cobs maintained higher L^* values (Fig. 1B) and lower of a^* and b^* values (Fig. 1C–D) than the CK group over time, indicating that DBD treatment delayed the loss of brightness, reddening and yellowing. SSC declined in both groups, but was higher in treated cobs than in untreated ones (Fig. 1E). DBD treatment also delayed weight loss compared with untreated cobs (Fig. 1F).

Metabolite profiles

Inter-sample correlation analysis showed good correlations among biological replicates (Fig. 1G). In CK-0d vs CK-8d, 1030 differentially accumulated metabolites (DAMs; 604 upregulated, 426 downregulated) were screened. Lipids (149; 99 upregulated, 50 downregulated), ketones/aldehydes/esters (142; 90 upregulated, 52 downregulated), and carbohydrates (102; 58 upregulated, 44 downregulated) accounted for high proportions. In CK-0d vs DBD-8d, we screened 966 DAMs (549 upregulated, 417 downregulated). They were dominated by lipids (142; 95 upregulated, 47 downregulated), ketones/aldehydes/esters (127; 79 upregulated, 48 downregulated), and organic acids (96; 52 upregulated, 44 downregulated). In CK-8d vs DBD-8d, we screened 250 DAMs (84 upregulated, 166 downregulated). They were dominated by lipids (32; 13 upregulated, 19

downregulated), ketones/aldehydes/esters (31; 7 upregulated, 24 downregulated), and terpenoids (28; 7 upregulated, 21 downregulated) (Fig. 1H, I; Table S1). 3,8-Di-O-methylellagic acid accumulated in CK-0d vs CK-8d, while 2-furanmethanol and 2-hydroxyhexanoic acid levels decreased. Trans-vaccenic acid and 12,13-dihome accumulated in CK-0d vs DBD-8d, while α-terpinene and 2-hydroxyhexanoic acid decreased. In CK-8d vs DBD-8d, trans-vaccenic acid and 2-furanmethanol accumulated, while 1-caffeoylquinic acid and 3,8-Di-O-methylellagic acid were substantially depleted (Fig. 1J). DAMs across the three comparisons were mostly enriched in D-amino acid metabolism, ABC transporters, histidine metabolism, and ascorbate and aldarate metabolism (Fig. S1A–C).

A total of 1196 DAMs were detected across the three comparisons (Fig. 2A; Table S2), dominated by lipids (14.97%), ketones/aldehydes/esters (13.04%), carbohydrates (9.36%), organic acids (9.03%), and terpenoids (8.44%). These metabolites are mainly involved in energy supply, membrane stability, and flavor formation, indicating that DBD treatment broadly regulated the postharvest metabolic homeostasis of sweet corn. K-means clustering of the 1196 DAMs divided them into two subclasses based on accumulation trends (Fig. 2B). Sub Class 1 (691 DAMs) comprised metabolites that progressively accumulated during senescence, dominated by lipids, ketones/aldehydes/esters, and terpenoids. This suggests close associations with postharvest membrane lipid oxidation and secondary metabolism activation. DBD treatment suppressed the accumulation of this subclass. Sub Class 2 (505 DAMs) was comprised of flavor- and nutrition-related metabolites, dominated by lipids, ketones/aldehydes/esters and amino acids that decreased after harvest. DBD treatment slowed their degradation and partially restored the levels of

some compounds by day 8 of storage. DBD treatment may therefore maintain sweet corn quality by regulating the synthesis and degradation rates of postharvest metabolites. It suppresses the enrichment of deterioration-related metabolites while slowing the consumption of flavor and nutritional compounds.

KEGG enrichment analysis showed that the three comparisons shared 12 KEGG pathways (Fig. 1K). DAMs associated with sphingolipid metabolism, zeatin biosynthesis, and glutathione metabolism were enriched in all comparisons. Venn analysis identified 123 DAMs common to all three comparisons (Fig. 2C): 132 were unique to CK-0d vs CK-8d, 113 unique to CK-0d vs DBD-8d, and 24 unique to CK-8d vs DBD-8d. In addition, CK-0d vs CK-8d shared 824 DAMs with CK-0d vs DBD-8d and 197 with CK-8d vs DBD-8d, while CK-0d vs DBD-8d shared 152 DAMs with CK-8d vs DBD-8d (Fig. 2C). Classifying the 123 common DAMs, ketones/aldehydes/esters accounted for the highest proportion (15.45%, 19), followed by organic acids (12.20%, 15) and terpenoids (11.38%, 14). Carbohydrates (8.94%, 11), lipids (8.94%, 11), and amino acids (6.50%, 8) also accounted for substantial proportions these DAMs (Fig. 2C; Table S3). These results indicate that DBD treatment induced changes in diverse metabolite classes, with ketones/aldehydes/esters and organic acids being the major classes involved in kernel quality regulation after harvest.

In summary, DBD treatment exerted bidirectional regulation of the sweet corn metabolism. The 1196 DAMs were dominated by lipids, ketones/aldehydes/esters, carbohydrates, organic acids, and terpenoids. K-means clustering showed that DBD treatment suppressed the enrichment of accumulation-type metabolites while alleviating the loss of depletion-type metabolites. The three comparisons were commonly enriched in

sphingolipid metabolism, zeatin biosynthesis, and glutathione metabolism, and the 123 common DAMs were dominated by ketones/aldehydes/esters, organic acids, and terpenoids.

Gene expression

PCA showed clear separation of the three sample groups along the principal component axes, indicating that DBD treatment induced marked differences in gene expression profiles (Fig. 2D). Pearson correlation analysis showed good correlations among samples within each group (Fig. 2E). Venn analysis identified 3306 DEGs unique to CK-0d vs CK-8d, 919 unique to CK-0d vs DBD-8d, and 678 unique to CK-8d vs DBD-8d. CK-0d vs CK-8d shared 7080 DEGs with CK-0d vs DBD-8d and 5092 with CK-8d vs DBD-8d, while CK-0d vs DBD-8d shared 2868 DEGs with CK-8d vs DBD-8d. A total of 2008 DEGs were common to all three comparisons (Fig. 2F).

CK-0d vs CK-8d yielded 13,470 DEGs (7652 upregulated, 5818 downregulated) (Fig. 2G), mainly enriched in starch and sucrose metabolism, pyruvate metabolism, glycolysis/gluconeogenesis, plant hormone signal transduction, and glutathione metabolism (Fig. S2A). CK-0d vs DBD-8d yielded 8859 DEGs (5274 upregulated, 3585 downregulated) (Fig. 2G), mainly enriched in phenylpropanoid biosynthesis, plant–pathogen interaction, MAPK signaling pathway–plant, starch and sucrose metabolism, and glycolysis/gluconeogenesis (Fig. S2B). CK-8d vs DBD-8d yielded 6630 DEGs (3365 upregulated, 3265 downregulated) (Fig. 2G), mainly enriched in phenylpropanoid biosynthesis, plant hormone signal transduction, starch and sucrose metabolism, MAPK signaling pathway–plant, and plant–pathogen interaction (Fig. S2C).

Carbohydrate and energy metabolism

Starch and sucrose metabolism and glycolysis/gluconeogenesis were enriched in both CK-0d vs CK-8d and CK-0d vs DBD-8d. This indicates that these two pathways play central roles in energy supply and soluble sugar homeostasis during storage of sweet corn. The decreased sweetness of sweet corn is mainly caused by respiratory consumption and the conversion of soluble sugars to starch (Ren et al., 2026). DBD treatment regulated starch and sucrose metabolism with the core goal of slowing sugar degradation and maintaining sweetness. On the one hand, DBD treatment prevented the senescence-associated downregulation of *α-glucosidase* (*AG*, NewGene_9739) and *trehalose 6-phosphate synthase* (*TPS*, LOC100285860), maintaining their expression levels. AG hydrolyzes oligosaccharides to glucose, ensuring monosaccharide supply and sufficient substrates for energy metabolism (Okuyama et al., 2016). TPS is a key enzyme in trehalose synthesis. Trehalose, as a non-reducing disaccharide, directly contributes sweetness while protecting proteins and membrane structures under postharvest stress (Eh et al., 2025). Maintaining its expression therefore enhanced sweetness perception and stress tolerance of the kernels. On the other hand, DBD treatment suppressed the abnormal postharvest upregulation of key genes for starch degradation and sugar conversion, a key mechanism for maintaining postharvest sweetness. DBD treatment repressed the upregulation of *α-amylase* (*AMY*, LOC100283908/LOC100383492/LOC103649884) and *β-amylase* (*BAM*, LOC103639137), which would result in slowing of excessive hydrolysis of starch to reducing sugars during storage. It also prevented soluble sugars from being rapidly consumed by respiration after a transient surge, thereby stabilizing kernel sugar content and sweetness quality (Zhao et al., 2024). *Phosphoglucomutase* (*PGM*, LOC103651489) catalyzes the interconversion of glucose-1-phosphate (G1P) and glucose-6-phosphate

(G6P) (Li et al., 2023). DBD treatment suppressed its abnormal upregulation, helping to alleviate postharvest sugar metabolism disorder and maintain glycolytic substrate homeostasis. In addition, DBD treatment repressed the upregulation of *starch synthase* (*SS*, LOC100101528). Repressed upregulation would avoid a futile cycle between starch synthesis and degradation, thereby reducing unnecessary energy and carbon consumption, and directing limited assimilates toward maintaining soluble sugar reserves (Fig. 3A).

In the glycolysis/gluconeogenesis pathway, DBD treatment restored the expression of genes for key glycolytic enzymes, ensuring stable energy supply. Specifically, DBD treatment upregulated the expression of *fructose-bisphosphate aldolase* (*FBA*, LOC542261), *glyceraldehyde-3-phosphate dehydrogenase* (*GAPDH*, LOC100037774/LOC542333), *pyruvate decarboxylase* (*PDC*, LOC542651/LOC542376), and *pyruvate, orthophosphate dikinase* (*PPDK*, LOC103635678). Such upregulation would allow the efficient conversion of glucose to pyruvate via glycolysis and ensure continuous ATP supply. Meanwhile, DBD treatment repressed over-expression of alcohol dehydrogenase (*ADH*, NewGene_2730) and related genes, which could reduce the conversion of sugars to ethanol under anaerobic conditions and avoid soluble sugar loss (Fig. 3B). DBD treatment also downregulated expression of the TCA cycle key genes *isocitrate dehydrogenase* (*IDH*, LOC100217128) and *aconitate hydratase* (*ACO*, LOC103647708), which would slow oxidation of glycolytic products by the TCA cycle, so that more carbon skeletons remained in the carbohydrate pool, supporting kernel sugar accumulation (Fig. 3C).

In the galactose metabolism pathway, DBD treatment maintained the expression of *α-glucosidase* (*AG*, NewGene_9739). The breakdown of maltose and oligosaccharides to

glucose would ensure continuous soluble sugar supply and sweetness replenishment. *Beta-galactosidase* (*BG*, LOC100191631/LOC103647648/LOC100383452) was likewise upregulated, promoting galactan hydrolysis and maintaining cell wall structural integrity. In addition, raffinose is an important osmotic regulator and soluble oligosaccharide (Nishizawa et al., 2008). *Raffinose synthase* (*RS*, LOC606463) was upregulated; increased raffinose synthesis can further enhance sugar reserves and stress tolerance of harvested sweet corn (Fig. 3D). In the fructose and mannose metabolism pathway, DBD treatment maintained the expression of *L-iditol 2-dehydrogenase* (*SDH*, LOC100283066) and *mannose-1-phosphate guanylyltransferase* (*GMPP*, LOC103651012), maintaining fructose–sorbitol metabolic balance. Both sorbitol and fructose are distinctly sweet sugar alcohols, and maintaining this balance helps preserve the characteristic refreshing sweetness of the kernels (Zhao et al., 2024). It also promotes mannose entry into nucleotide sugar metabolism, providing substrates for glycoprotein and cell polysaccharide synthesis (Engel et al., 2012). Meanwhile, DBD treatment repressed the upregulation of *xylose isomerase* (*XylA*, LOC100381992). This reduced the formation of abnormal pentose metabolic branches, maintained hexose metabolism stability, and avoided the wasteful diversion of hexoses to non-sweet pentose pathways (Fig. 3E). In summary, DBD treatment suppressed excessive postharvest carbohydrate breakdown senescence. While slowing starch degradation and respiratory consumption, DBD treatment restored the functional activities of sugar synthesis and conversion enzymes. As a result, postharvest soluble sugar content and sweetness quality of sweet corn would be maintained.

Cell wall metabolism

Cell wall structural integrity directly affects the firmness, weight loss, and texture of postharvest sweet corn. In the pentose and glucuronate interconversions pathway, DBD treatment regulated multiple key nodes. Compared with the CK group, *sorbitol dehydrogenase* (*SDH*, LOC100283066) expression recovered significantly after DBD treatment, favoring the efficient conversion of sorbitol to fructose and avoiding excessive intracellular sorbitol accumulation. *Pectinesterase* (*PME*, LOC100273304) was continuously upregulated during senescence, and DBD treatment downregulated its expression, which would inhibit excessive pectin demethylesterification. *Xylose isomerase* (*XylA*, LOC100381992) was upregulated during senescence but downregulated after DBD treatment. Excessive diversion through the pentose phosphate pathway would be avoided, thereby maintaining NADPH supply and nucleotide sugar precursor synthesis balance, and indirectly supporting normal hemicellulose assembly. *Glucuronokinase* (*GlcAK*, LOC103648024) was downregulated during senescence, and DBD treatment restored its expression. This ensured normal glucuronate cycle operation and provided sufficient precursors for cell wall polysaccharide synthesis (Fig. 3F).

DBD treatment repressed lignin synthesis in the phenylpropanoid biosynthesis pathway. Inhibited lignin synthesis would block the excessive activation of phenylpropanoid metabolism during senescence, thereby delaying kernel hardening caused by excessive lignin deposition. Basal pathway activity was retained to maintain antioxidant defense and moderate cell wall structural reinforcement. *Phenylalanine ammonia-lyase* (*PAL*, LOC100381820), encoding the entry rate-limiting enzyme of the phenylpropanoid pathway, was sharply upregulated during senescence. After DBD treatment its expression remained above CK-0d levels but was downregulated in the CK-8d vs DBD-8d

comparison, reducing the oversupply of downstream lignin synthesis substrates. *Shikimate O-hydroxycinnamoyltransferase* (*HCT*, LOC103654324/LOC109942262) was greatly upregulated during senescence. catalyzes the esterification of p-coumaroyl-CoA with shikimate/quinate and is a key node linking the phenylpropanoid pathway to phenolic acid synthesis such as chlorogenic acid (Chen et al., 2026b). Upregulation of *HCT* would provide abundant intermediates for downstream lignin monomer synthesis as well as promot phenolic acid accumulation. DBD treatment reduced the upregulation of *HCT* upregulation, which would decrease the excessive diversion of phenolic acids toward lignin. *Caffeic acid 3-O-methyltransferase* (*COMT*, LOC100283243) was upregulated during senescence. COMT catalyzes the methylation of caffeic acid to ferulic acid and participates in the methylation modification of lignin monomers (Liu et al., 2026). DBD treatment decreased the upregulation of *COMT*, which would reduce excessive synthesis of guaiacyl and syringyl lignin. *Cinnamyl-alcohol dehydrogenase* (*CAD*, LOC113839551) was upregulated during senescence, catalyzing the reduction of cinnamaldehydes to cinnamyl alcohols, a key step in lignin monomer biosynthesis (An et al., 2024). DBD treatment decreased the upregulation of *CAD*, which would reduce cinnamyl alcohol monomers and limit substrate accumulation for lignin polymerization at the source. *Peroxidase* (*POD*, LOC100194008/LOC100216644) was strongly upregulated during senescence. POD is the final enzyme of lignin polymerization, catalyzing the oxidative cross-linking of cinnamyl alcohol monomers into lignin macromolecules, and thereby directly causing cell wall lignification and kernel hardening (Warinowski et al., 2016). DBD treatment reduced *POD* upregulation, which would prevent excessive lignin deposition in the cell wall. Thus, by regulating gene expression in the phenylpropanoid–

lignin synthesis pathway, DBD treatment suppressed excessive lignin deposition and delayed kernel hardening. As a result, kernel firmness and good eating quality of sweet corn is maintained during storage (Fig. 3G).

Antioxidant and secondary metabolism

Phenylpropanoid biosynthesis, glutathione metabolism, and ascorbate and aldarate metabolism were highly enriched in the DBD group. This reveals the mechanisms by which DBD treatment enhances antioxidant capacity and defense systems.

In the primary antioxidant system, the glutathione metabolism pathway, *spermidine synthase* (*SPE*, LOC732743) was upregulated. As a result, spermidine synthesis capacity would be maintained, MDA accumulation suppressed, and s membrane lipid peroxidationreduced. The g*lutathione S-transferase (GST)* family showed the most pronounced DBD-responsive upregulation: LOC541848, LOC541836, and LOC541850 were coordinately upregulated, enhancing antioxidant capacity and promoting ROS scavenging. LOC542311 was reversed from downregulation to upregulation, and the downregulation of LOC541838 and LOC542634 was attenuated, coordinately restoring the functional balance of the GST family (Table S4). In the ascorbate and aldarate metabolism pathway, DBD treatment optimized the redox balance of ascorbic acid. Upregulation of *L-ascorbate oxidase* (*AO*, LOC100273169) by DBD treatment would favor inhibition of the oxidative conversion of ascorbic acid to dehydroascorbic acid and slow the degradation of ascorbic acid. *L-galactono-1,4-lactone dehydrogenase* (*GLDH*, LOC103636542) recovered from a highly expressed state to moderate expression, favoring the maintenance of ascorbic acid synthesis capacity. The downregulation of *glucuronokinase* (*GlcAK*,

LOC103648024) was suppressed and restored to a moderate level, providing precursor support for the glucuronate pathway (Table S4).

DBD treatment coordinately regulated the synthesis of terpenoid backbones, monoterpenes, and diterpenes in the terpenoid biosynthesis pathway, which would optimize the production and allocation of defensive terpenoids while maintaining t hormone balance during storage. At the terpenoid backbone synthesis level, *hydroxymethylglutaryl-CoA reductase* (*HMGR*, LOC103627645) recovered from low expression to a moderate state, ensuring terpenoid precursor supply. *Farnesyl diphosphate synthase* (*FDPS*, LOC541903) recovered from downregulation, providing precursors for sesquiterpene and triterpene defense compounds. *Diphosphomevalonate decarboxylase* (*MVD*, LOC103643980) fell back from abnormally high expression to normal levels, restoring homeostasis. *4-hydroxy-3-methylbut-2-en-1-yl diphosphate reductase* (*LytB*, NewGene_14511) was tuned from abnormally high expression back to a moderate level. As a result, the catalytic efficiency of the terminal reductive step of the MEP pathway and the synthesis homeostasis of isopentenyl diphosphate (IPP) and dimethylallyl diphosphate (DMAPP) would be maintained (Fig. 4A). Expression of *(E)-8-carboxylinalool synthase* (*8-CLS*, LOC103633567) involved in monoterpene synthesis was further increased by DBD treatment, promoting the synthesis and release of linalool-type monoterpenes. As a result, pathogen defense would be enhanced while aromatic quality would be maintained (Fig. 4B). Expression of *ent-copalyl diphosphate synthase* (*ent-CPS*, gene-an1) involved in diterpene synthesis and providing precursors for gibberellins and phytoalexins, recovered from downregulation. *Oryzalexin E synthase* (*CYP76M6*, LOC100273519) recovered from a high-level state to a moderate level, maintaining diterpene phytoalexin

synthesis capacity. The DBD-induced upregulation of *trimethyltridecatetraene synthase* (*CYP92C6*, LOC103631958) was repressed, which would reduce excessive synthesis of tridecatetraene volatile terpenes. Excessive carbon diversion to defensive volatiles would be avoided and the retention of nutrients such as soluble sugars favored. *Gibberellin 2beta-dioxygenase* (*GA2ox*, NewGene_16448/NewGene_3666) recovered from the abnormally high levels induced by postharvest senescence to a moderate state. As a result, GA metabolic homeostasis would be maintained and excessive inactivation of GA avoided, thereby delaying senescence-related quality deterioration such as kernel yellowing of sweet corn (Fig. 4C). Overall, DBD treatment suppressed the stress-induced overactivation of antioxidant genes while restoring the expression of core synthetic enzymes, thereby maintaining redox and hormone homeostasis.

Hormone signaling and defense pathways

The plant hormone signal transduction pathway was enriched, indicating that the DBD treatment systematically regulated postharvest senescence and stress responses of sweet corn. Within this pathway, DBD treatment optimized hormone balance and stress responses (Fig. 4D). DBD treatment suppressed ethylene signal transduction and thereby alleviated ethylene-mediated postharvest senescence as indicated by lower expression of the *ethylene receptor* (*ETR*, LOC103633258/LOC103654807). DBD treatment repressed the expressions of *ethylene-insensitive protein 2* (*EIN2*, LOC103643855) and *ethylene-insensitive protein 3* (*EIN3*, LOC103653667), coordinately blocking downstream ethylene responses. Meanwhile, *serine/threonine-protein kinase CTR1* (*CTR1*, LOC100304418) expression recovered from low levels, as did that of *EIN3-binding F-box protein* (*EBF1/2,* LOC100281166), coordinately reinforcing the shutdown of ethylene signaling.

DBD treatment resulted in the regulation of abscisic acid (ABA) signal transduction. The *abscisic acid receptor PYL family* (*PYL*, LOC100280849/LOC100273048) was expressed at very low levels during senescence but recovered after DBD treatment compared with CK-8d. This moderately maintained ABA perception capacity. The *ABA responsive element binding factor* (*ABF*, LOC103637889) was downregulated during senescence but increased after DBD treatment compared with CK-8d. This favored the retention of transcriptional responsiveness to stress. In contrast, *serine/threonine-protein kinase SRK2* (*SnRK2*, LOC100281258) was downregulated from its high expression during senescence. Downregulation wouldattenuate ABA signal amplification and thereby slow senescence.

Brassinosteroid (BR), gibberellin (GA), and auxin signal transduction were coordinately strengthened after DBD treatment. Four *brassinosteroid insensitive 1-associated receptor kinase 1* (*BAK1*, LOC103654758/LOC103633392/LOC103632842/LOC100284829) genes and downstream *brassinosteroid resistant 1/2* (*BZR1/2*, LOC100194109) were upregulated, though not restored to day-0 levels. *Xyloglucan:xyloglucosyl transferase TCH4* (*TCH4*, LOC542312) also increasedindicating that DBD treatment initiated BR signal transmembrane transduction but was insufficient to fully reverse senescence. The *gibberellin receptor GID1* (*GID1*, LOC103631970) shifted from downregulation to recovery, maintaining GA signal perception. Expression of the *SAUR family protein* (*SAUR*, LOC103642058) recovered, indicating that DBD treatment activated downstream auxin signaling and partially restored auxin responsiveness.

Integrated transcriptomic and metabolomic analysis

DEGs and DAMs were enriched in the top 10 KEGG pathways across the three comparisons were analyzed. Starch and sucrose metabolism and glycolysis/gluconeogenesis were enriched in both CK-0d vs CK-8d and CK-0d vs DBD-8d, representing the core metabolic processes during storage (Fig. 5A–C). Glutathione metabolism was enriched in all three comparisons and was cross-validated by metabolomic data, indicating that this pathway continuously regulated by DBD treatment. In addition, ascorbate and aldarate metabolism was enriched in CK-8d vs DBD-8d. This suggests that DBD treatment may maintain redox homeostasis by regulating ascorbic acid metabolism at the late senescent stage. Based on these analyses, starch and sucrose metabolism, glutathione metabolism, and ascorbate and aldarate metabolism were further subjected to integrated analysis.

In CK-0d vs CK-8d, five core carbohydrate DAMs in the starch and sucrose metabolism pathway (cellobiose, isomaltose, maltose, sucrose, and uridine 5'-diphospho-D-glucose) were positively correlated with each other. All were positively correlated with *BGS*, *AG*, and *TPS* but negatively correlated with *AMY*, *BAM*, *EBG*, *PGM*, and *SS* (Fig. 5D). The slightly higher proportion of negative correlations indicated enhanced carbohydrate catabolism during senescence. In the CK-0d vs DBD-8d comparison, four core carbohydrate DAMs (cellobiose, isomaltose, maltose, and uridine 5'-diphospho-D-glucose) were positively correlated with each other. All were positively correlated with *BGS*, *AG*, and *TPS* but negatively correlated with *AMY*, *BAM*, *EBG*, *PGM*, and *SS* (Fig. 5E). Compared with CK-0d vs CK-8d, the proportions of positive and negative correlations tended to balance, and sucrose was not detected as a DAM in this comparison. These effects suggest that DBD treatment can reduce carbohydrate catabolism during sweet corn

senescence. Specifically, DBD treatment may maintain the levels of soluble sugars such as sucrose and slow senescence. It may do so by repressing the expression of starch and sucrose degradation genes such as *AMY*, *BAM*, and *EBG*. At the same time, it maintains the activities of sugar synthesis genes such as *BGS*, *AG*, and *TPS*. In addition, uridine 5'-diphospho-D-glucose, as a glycosyl donor (Zhang et al., 2025a), may accumulate to favor the synthesis and repair of cell wall polysaccharides.

Further association analysis of the two specifically enriched antioxidant pathways in CK-8d vs DBD-8d revealed that in the ascorbate and aldarate metabolism pathway, L-ascorbic acid was negatively correlated with D-glucuronic acid lactone, and both were negatively correlated with *AO* and *GLDH* but positively correlated with *GlcAK*. Thes effects suggest that DBD treatment may maintain ascorbic acid accumulation by promoting synthesis and inhibiting degradation. However, whether product feedback regulation of synthetic enzymes exists remains difficult to conclude from correlation data alone. In the glutathione metabolism pathway, one DAM, L-ascorbic acid, was identified. It was negatively correlated with *IDH* and *SPE* but positively correlated with *GST*, reflecting the reallocation of antioxidant resources between the AsA and GSH systems. When AsA system activity is enhanced, dependence on the GSH system decreases accordingly (Fig. 5F). In summary, DBD treatment can systematically activate the AsA–GSH coordinated antioxidant network of sweet corn.

Protein abundance

CK-0d vs CK-8d identified 940 unique proteins (DEPs; 474 upregulated, 466 downregulated). CK-0d vs DBD-8d identified 765 DEPs (397 upregulated, 368 downregulated), and CK-8d vs DBD-8d identified 71 DEPs (34 upregulated, 37

downregulated) (Fig. 6A). Venn analysis showed 321 DEPs unique to CK-0d vs CK-8d, 163 unique to CK-0d vs DBD-8d, 23 unique to CK-8d vs DBD-8d. A total of 15 DEPs were common to all three comparisons (Fig. 6B). Functional annotation indicated that these 15 proteins mainly participate in redox regulation, lipid metabolism, and stress and defense responses. Examples include short chain dehydrogenase, FAD binding domain, probable lipid transfer proteins, cytochrome P450, and UDP-glucosyl transferase. They displayed different expression patterns across comparisons. In CK-0d vs CK-8d and CK-0d vs DBD-8d, most of these proteins were upregulated, particularly those related to stress responses and secondary metabolism. In CK-8d vs DBD-8d, however, most core proteins showed opposite regulatory trends. Proteins upregulated during senescence were suppressed by DBD treatment (downregulated in CK-8d vs DBD-8d), while proteins downregulated during senescence were rescued by DBD treatment (upregulated) (Table S5). This indicates that DBD treatment maintained the relative stability of these protein expression levels. The KEGG pathway enrichment bubble plot showed the most enriched pathways in CK-0d vs CK-8d. They included phenylpropanoid biosynthesis, other glycan degradation, butanoate metabolism, ribosome, and biosynthesis of unsaturated fatty acids (Fig. S2D). The top enriched pathways in CK-0d vs DBD-8d included phenylpropanoid biosynthesis, butanoate metabolism, linoleic acid metabolism, other glycan degradation, and biosynthesis of unsaturated fatty acids (Fig. S2E). The most enriched pathways in CK-8d vs DBD-8d included phenylalanine metabolism, flavone and flavonol biosynthesis, cutin/suberine and wax biosynthesis, isoquinoline alkaloid biosynthesis, and phenylpropanoid biosynthesis (Fig. S2F).

COG classification of DEPs across the three comparisons showed that the highest-proportion categories in CK-0d vs CK-8d were lipid transport and metabolism, posttranslational modification/protein turnover/chaperones, translation/ribosomal structure and biogenesis, carbohydrate transport and metabolism, and general function prediction only (Fig. 6C). In CK-0d vs DBD-8d, the top categories were carbohydrate transport and metabolism, posttranslational modification/protein turnover/chaperones, general function prediction only, lipid transport and metabolism, and energy production and conversion (Fig. 6D). DEPs in CK-8d vs DBD-8d were mainly distributed in amino acid transport and metabolism, posttranslational modification/protein turnover/chaperones, general function prediction only, defense mechanisms, and energy production and conversion (Fig. 6E). Pfam annotation revealed differences in protein expression patterns among the three comparisons. In CK-0d vs CK-8d, UDP-glucuronosyl and UDP-glucosyl transferase family proteins were the most abundant, followed by RNA recognition motif-containing proteins, cytochrome P450 family proteins, and glutathione S-transferase family proteins. Therefore, senescence mainly involved changes in proteins related to secondary metabolism, stress responses, and post-translational modifications (Fig. 6F). In CK-0d vs DBD-8d, UDP-glucuronosyl and UDP-glucosyl transferase family proteins remained the most abundant, along with glutathione S-transferase family proteins, cellulose synthase, and 14-3-3 proteins. This indicates that DBD treatment affected proteins related to secondary metabolism, stress defense, cell wall synthesis, and signal transduction (Fig. 6G). In CK-8d vs DBD-8d, the protein counts per family were markedly lower, with probable lipid transfer proteins, Hsp20/alpha crystallin family proteins, and aromatic amino acid lyases being the most abundant. This indicates that DBD treatment specifically

474 altered proteins related to lipid transport, stress responses, and aromatic amino acid
475 metabolism in the late storage stage (Fig. 6H).

476 To further explore how DBD treatment regulates sweet corn quality in the late
477 senescence stage, we systematically classified the 71 DEPs identified in the CK-8d vs
478 DBD-8d comparison. The classification was based on Pfam domain annotation and
479 biological function. Seventeen DEPs were classified as stress- and defense-related. The
480 most significantly downregulated ones included glutathione peroxidase (GPX), glutathione
481 S-transferase P (GST P), thioredoxin (Trx), glutaredoxin, cytochrome P450, and TB2/DP1
482 (HVA22 family). The most significantly upregulated ones included Hsp20/alpha crystallin
483 family, peroxidase, probable lipid transfer protein, stress responsive A/B Barrel Domain-
484 containing protein, and chaperonin 10 Kd subunit. Nineteen were classified as energy and
485 substance metabolism-related. The most significantly downregulated ones included
486 putative serine esterase, elongation factor Tu GTP binding domain, subtilase family,
487 aromatic amino acid lyase, and acetyltransferase (GNAT) family. The most significantly
488 upregulated ones included creatine kinase M-type, NAD-dependent glycerol-3-phosphate
489 dehydrogenase, and oxysterol-binding protein. Twelve were classified as cell structure-
490 and senescence-related, with the most significantly upregulated ones including probable
491 lipid transfer proteins, peptidase inhibitor I9, and C-terminus of histone H2A. Twelve were
492 classified as transcription- and translation-related. The most significantly downregulated
493 ones included KH domain-containing protein, PPR repeat family protein, LUC7
494 N_terminus-containing protein, and Dos2-interacting transcription regulator. The most
495 significantly upregulated included PLATZ transcription factor, transcription factor TFIIB
496 repeat, Hsp70-interacting protein N-terminal domain, and ubiquitin-conjugating enzyme.

The remaining 11 were novel genes or unannotated proteins whose biological functions require further investigation (Table S6).

Multi-omics integration reveals mechanisms underlying DBD plasma-delayed postharvest senescence in sweet corn

The three-omics KEGG co-enrichment bubble plot showed significant cross-omics consistency in CK-0d vs CK-8d. Phenylpropanoid biosynthesis and starch and sucrose metabolism were enriched at all three omics levels. In addition, glutathione metabolism, sphingolipid metabolism, galactose metabolism, and valine, leucine and isoleucine degradation were also enriched at all three omics levels. The metabolomic enrichment factor of flavone and flavonol biosynthesis approached 1.0, but the transcriptomic signal was weak. This suggests that flavonol metabolism during natural senescence may be mainly driven by post-translational regulation or metabolite homeostasis mechanisms (Fig. S3A). In CK-0d vs DBD-8d, phenylpropanoid biosynthesis remained the core pathway with the most consistent three-omics response. Compared with CK-0d vs CK-8d, defense-related pathways including isoquinoline alkaloid biosynthesis, ascorbate and aldarate metabolism, and cyanoamino acid metabolism entered the co-enrichment list (Fig. S3B). In CK-8d vs DBD-8d, the co-enriched pathways decreased to tyrosine metabolism, ascorbate and aldarate metabolism, and glutathione metabolism (Fig. S3C). Ascorbate and aldarate metabolism and glutathione metabolism were enriched at all three omics levels in both CK-0d vs DBD-8d and CK-8d vs DBD-8d, suggesting that DBD treatment activated the AsA–GSH antioxidant system.

To elucidate how DBD treatment induces antioxidant defense in the late storage stage, we performed integrated analysis of ascorbate and aldarate metabolism and glutathione

metabolism at the KEGG pathway level. In the ascorbate and aldarate metabolism pathway (Fig. 7A), upstream precursors such as UDP-D-glucose and D-glucuronate-1P were downregulated during senescence. The end product L-ascorbate decreased synchronously, while D-galactaro-1,5-lactone was upregulated, suggesting an insufficient precursor supply for ascorbic acid synthesis during senescence and a blockage of metabolic flux from D-galactaro-1,5-lactone to L-ascorbate. DBD treatment maintained the relative stability of these metabolites, slowing the decline in ascorbic acid content. At the gene level, *GlcAK* (LOC103648024) was highly downregulated during senescence, and DBD treatment suppressed this downregulation with partial recovery of expression. This favors the metabolic flux of D-glucuronate toward phosphorylation. *AO* (LOC100273169) and *GLDH* (LOC103636542, LOC103653136) were abnormally highly expressed during senescence. DBD treatment resulted in more moderate levels, favoring the avoidance of excessive oxidation and synthetic consumption of L-ascorbic acid. By restoring silenced genes and tuning back overactivated genes, DBD treatment maintained L-ascorbic acid synthesis capacity while reducing its degradative losses. In the glutathione metabolism pathway (Fig. 7B), L-ornithine and L-ascorbic acid were decreased during senescence. DBD treatment resulted in upregulation of *SPE*, *GST* (LOC541848, LOC541836, LOC541850), and LOC542311 during senescence. LOC541838 and LOC542634 partially recovered from deep silencing. The *GST* family thus coordinately enhanced ROS scavenging and detoxification capacity. The three-omics coordinated regulation of the AsA–GSH pathway was highly consistent with physiological indicators. DBD treatment maintained higher L-ascorbic acid content and ROS scavenging capacity. These effects are consistent with those of quality indicators such as reduced weight loss, maintained

firmness, and preserved color. Activation of the glutathione metabolic system provided cells with multi-layered redox buffering, thereby alleviating oxidative senescence at the late storage stage. In summary, in the late storage stage, DBD treatment restored precursor-supply genes (*GlcAK*) and increased *GST* family gene expression. Expression of catabolic genes (*AO*, *GLDH*) was reduced, which would enhance the ascorbate–glutathione antioxidant system and ultimately coordinate optimization of antioxidant defense at the transcript, protein, and metabolite levels.

Discussion

The loss of sweetness in harvested sweet corn mainly stems from high respiratory metabolism during which soluble sugars such as sucrose are rapidly consumed. In addition, some cultivars undergo complex changes involving sugar-to-starch conversion or starch hydrolysis to sugars (Becerra-Sanchez and Taylor, 2021; Mushtaq et al., 2025). Applications of cold plasma to other fruit and vegetables have shown that it can affect postharvest sugar metabolism by intervening in respiratory metabolic pathways. For example, He et al. (2025b) found that the activities and gene expression of glycolysis–TCA cycle (EMP-TCA) related enzymes in apricot fruit after cold plasma treatment were suppressed. In addition, respiration rates and sugar consumption were reduced. In our study, DBD regulation of sugar metabolism was characterized by suppressing degradation, maintaining synthesis, and optimizing energy allocation. The expression of starch degradation genes such as *AMY* and *BAM* was repressed after DBD treatment, which would slow hydrolysis of starch to reducing sugars during storage and prevent soluble sugars from being rapidly consumed by respiration after a transient surge. Meanwhile, genes maintaining sugar homeostasis such as *AG* and *TPS* maintained relatively normal

expression levels. These findings are consistent with those of Li et al. (2024) who found that differential expression of postharvest sugar metabolism genes in different sweet corn cultivars affected quality, and Chen et al. (2027), who reported similar effects in microwave-treated corn.

DBD treatment maintained the expression of key glycolytic enzymes such as FBA and GAPDH while downregulating TCA cycle genes such as *IDH* and *ACO*. Glycolysis partially recovered while respiratory consumption by the TCA cycle was suppressed, and overall respiratory consumption decreased. This is broadly consistent with the observation of He et al. (2025b) that cold plasma downregulated the EMP-TCA cycle and suppressed respiratory metabolism in apricot fruit. The effect of DBD treatment on postharvest sugar metabolism of sweet corn is therefore not simple metabolic stasis but a shift from rapid consumption to relatively conservative maintenance. This explains why the DBD group showed slower SSC decline and lower weight loss.

Postharvest softening of most fruit and vegetables is mainly associated with enhanced activities of cell wall degrading enzymes such as *PME*, *PG*, and *XTH*. This leads to cell wall loosening and texture softening (Nikzadfar et al., 2024). Unlike the softening of most fruit and vegetables, sweet corn kernels increase in firmness during storage. Liu et al. (Liu et al., 2024b) and Wang et al. (Wang et al., 2024a) both reported continuous increases in kernel firmness of postharvest sweet corn. This increase is related to cell wall shrinkage caused by water loss, pectin changes, and possible lignin accumulation. The firmness increase of sweet corn during storage shares mechanistic similarities with postharvest lignification-induced hardening of bamboo shoots (Wu et al., 2023). A similar hardening occurs in postharvest loquat flesh (Huang et al., 2023b). Wu et al. (Wu et al., 2023) found

589 that DBD treatment of bamboo shoots delayed the hardening process by inhibiting PME
590 and β-Gal activities and regulating cellulose and lignin accumulation. Zhang and Cheng
591 (2024) reported that genes encoding cell wall degrading enzyme genes such as *PG*, *PE*,
592 *BGAL*, *PL*, and *XTH* were downregulated, and softening slowed, in blueberries after cold
593 plasma treatment. These results indicate that DBD regulation of cell wall metabolism
594 shares common features across species, with slowed softening associated with inhibition
595 of cell wall degrading enzymes, and delayed hardening by intervening in cell wall synthesis
596 and cross-linking. In our study, DBD treatment delayed the firmness increase of sweet
597 corn. At the cell wall degradation level, *PME* expression was repressed after DBD
598 treatment, reducing cell wall loosening and subsequent cross-linking hardening caused by
599 excessive pectin demethylesterification. The phenylpropanoid biosynthesis pathway is
600 another key node regulating kernel hardening. During senescence, genes such as *PAL*,
601 *HCT*, *COMT*, were upregulated; as a result increased synthesis of lignin monomers and
602 excessive deposition in the cell wall, would cause kernel hardening. DBD treatment
603 suppressed upregulation of these genes. Although *PAL* remained above initial levels, it was
604 reduced in the CK-8d vs DBD-8d comparison. The upregulation magnitudes of *HCT*,
605 *COMT*, and *CAD* were reduced, decreasing the excessive diversion of phenolic acids
606 toward lignin and the oversupply of cinnamyl alcohol monomers. The upregulation of *POD*
607 was repressed, blocking the excessive cross-linking of lignin macromolecules in the cell
608 wall. This regulatory pattern is similar to that described by Wu et al. (2023) for bamboo
609 shoots, where DBD delayed hardening by inhibiting cell wall metabolism. The
610 phenylpropanoid pathway sits at the intersection of structural and antioxidant metabolism
611 (Mehravi et al., 2025), and its products are involved in moderate cross-linking of the cell

612 wall to enhance mechanical stability (Xiao et al., 2025). The products also provide
613 precursors for the synthesis of antioxidant substances such as flavonoids and chlorogenic
614 acid (Tang et al., 2021). DBD regulation of the phenylpropanoid pathway may therefore
615 produce two effects simultaneously. On the one hand, by inhibiting the overactivation of
616 the *PAL–HCT–COMT–CAD–POD* cascade, it reduces hardening caused by excessive
617 lignin deposition in the cell wall while maintaining basic structural integrity. On the other
618 hand, by retaining basal pathway activity, it allows partial carbon flux to be diverted to the
619 synthesis of phenolic antioxidants such as chlorogenic acid. Carbon flux therefore does not
620 flow entirely into the lignin branch. This differs from the mechanism of conventional
621 modified atmosphere packaging (MAP), which indirectly slows cell wall degradation by
622 lowering oxygen concentration to suppress respiration. Although MAP can maintain sweet
623 corn firmness to some extent, it is greatly affected by temperature fluctuations, and cannot
624 precisely regulate the expression of cell wall metabolism genes (Liu et al., 2021). In
625 contrast, DBD treatment more directly intervened in the balance of cell wall synthesis and
626 degradation gene expression while linking antioxidant metabolism. This also explains why
627 the DBD group showed both moderated firmness changes and better maintained color and
628 other quality attributes. These outcomes directly reflect the coordinated changes in cell
629 wall and antioxidant metabolism.

630 In postharvest senescence of fruit and vegetables, oxidative damage caused by ROS
631 accumulation importantly drives quality deterioration (Huang et al., 2023a; Zhang et al.,
632 2026; Zhang et al., 2025b). However, the effect of DBD treatment on the antioxidant
633 system is not simply enhancement or suppression but presents rather complex
634 characteristics. At the transcriptomic level, multiple members of the *GST* family in

glutathione metabolism were upregulated. In ascorbic acid metabolism, the precursor-supply gene *GlcAK* recovered expression while the catabolic genes *AO* and *GLDH* were repressed. This indicates that DBD treatment may activate antioxidant defenses (Teng et al., 2025). However, the proteomic results showed a different trend: in the CK-8d vs DBD-8d comparison, core antioxidant proteins such as GPX, GST P, and Trx were downregulated. That is, their abundances were lower in the DBD group than in the CK group. The differential response between transcript and protein levels may stem from the intrinsic characteristics of DBD treatment itself. The RONS generated by DBD are highly reactive. They can directly oxidize thiol groups and aromatic amino acid residues of proteins, thereby causing conformational changes or accelerating their degradation (Huang et al., 2023a). Meanwhile, after sensing exogenous oxidative stress, cells may reduce translation efficiency through negative feedback regulation to avoid energy expenditure caused by excessive responses (Abu Siam et al., 2026). In addition, there is an inherent delay between transcription and protein synthesis as gene transcription peaks often precede protein synthesis peaks, and protein turnover rates differ markedly from mRNA half-lives. By the day 8 sampling point, therefore, some proteins may not have maintained high concentrations due to oxidative damage or accelerated turnover (Bai et al., 2021; Lecourieux et al., 2020). Overall, these results suggest that the effect of DBD treatment on the antioxidant system of sweet corn is not simply an enhancement of enzymatic antioxidant capacity. It more likely involves direct participation of exogenous RONS in redox balance. It also involves the induction of non-enzymatic antioxidant accumulation to maintain homeostasis (Nikzadfar et al., 2024; Zhang and Cheng, 2024). The metabolomic data revealed that the DBD treated sweet corn accumulated more flavonoids,

alkaloids, and other phenolic substances than CK group. This finding also supports the existence of a compensatory shift between enzymatic and non-enzymatic antioxidant systems. When endogenous antioxidant enzyme protein levels were not elevated, cells compensated for the defense gap by accumulating small-molecule phenolics. As a result, oxidative homeostasis is achieved (Zhang et al., 2026; Zhang et al., 2023).

Plant hormones act by affecting upstream signals that regulate postharvest senescence, and their balance directly determines the direction of downstream metabolic pathways (Shi et al., 2024; Wang et al., 2025). In this study, DBD treatment systematically adjusted the hormone signaling network of sweet corn, providing important clues for understanding the changes in sugar metabolism, cell wall metabolism, and antioxidant pathways. Ethylene is a key factor regulating changes in color, texture, aroma, flavor, and nutrients during fruit ripening (Liu et al., 2024a). In the ethylene signaling pathway, the expression of the receptor gene *ETR* and downstream transducers *EIN2* and *EIN3* was repressed. Meanwhile, the expression of the negative regulators *CTR1* and *EBF1/2* partially recovered, indicating that ethylene signal transmission was blocked (Liu et al., 2024a). In the ABA signaling pathway, *PYR*/*PYL*/*RCAR* receptors perceive ABA and form a ternary complex with *PP2C*. This releases and activates *SnRK2*, which in turn phosphorylates downstream transcription factors such as *ABF* (Pizzio, 2025). In this study, DBD treatment restored the expression of the ABA receptor *PYL* and the response factor *ABF,* which would preserve a certain level of stress perception capacity. At the same time, it downregulated the expression of the signal amplifier *SnRK2* to prevent excessive activation of the senescence program. This "restore perception, suppress amplification" pattern resembles the negative feedback regulation observed in postharvest citrus fruit ABA

signalosome studies (Romero et al., 2012). They found that when ABA levels increase, *PYL* expression is downregulated while *PP2C* (a negative regulator) is upregulated to reset the signaling pathway. The differential regulation of *PYL* and *SnRK2* by DBD treatment may follow a similar feedback logic, delaying senescence while retaining the basic responsiveness of the cell to adversity. In addition, growth-promoting hormone signals such as BR, GA, and auxin also recovered to varying degrees. The restored expression of *BAK1* and *BZR1/2* (BR signaling), *GID1* (GA receptor), and the *SAUR* family (downstream of auxin) formed an antagonistic balance. It countered the weakened senescence-promoting signals of ethylene and ABA. Balanced adjustment among hormone signals may underlie the coordinated adjustment of downstream sugar metabolism, cell wall metabolism, and antioxidant pathways toward delayed senescence (Yan et al., 2024). DBD treatment not only affected the metabolic action but also intervened, through oxidative signals, in how plants perceive and respond to the postharvest environment.

The value of multi-omics integration lies in identifying the core pathways commonly pointed to by numerous differential changes. Integrating transcriptomic, proteomic, and metabolomic data has proven to be an effective strategy for identifying key metabolic hubs regulating postharvest quality (Storch et al., 2025; Wang et al., 2024b), and dedicated cross-species multi-omics platforms such as FVRS now provide additional resources for comparative studies of fruit and vegetable ripening and senescence (Ma et al., 2026). In this study, the AsA–GSH metabolic pathway was one of the few pathways that was consistently enriched at the transcriptome, proteome, and metabolome levels indicating that it is the core pathway through which DBD regulates postharvest quality of sweet corn. This view is supported by the induction of the endogenous antioxidant defense system of

apricots by generating RONS (He et al., 2025a). Moderate oxidative stress can enhance AsA–GSH cycle efficiency, thereby converting external stress signals into protective physiological responses. From the perspective of metabolic network topology, the AsA–GSH pathway is linked upward to carbohydrate metabolism and cell wall synthesis precursor supply via the glucuronate pathway. For example, D-galacturonic acid is both a component of cell wall pectin and an alternative entry point for AsA synthesis (Ifigeneia et al., 2021). Meanwhile, nucleotide sugar precursors such as GDP-mannose are shared substrates for cell wall polysaccharide and AsA synthesis (Linster and Clarke, 2008), which tightly coupled with the AsA–GSH cycle through GST family proteins, coordinately maintaining cellular redox homeostasis (Decros et al., 2019). A transcriptomic study of postharvest mango similarly observed coordinated differential expression patterns (Tahir et al., 2024), with both GST family members and key AsA–GSH cycle enzyme genes responding to oxidative stress. The quality improvements in sweet corn during storage were highly coordinated with the activation of the AsA–GSH pathway. These improvements included greater sugar retention, slower water loss, brighter color, and more tender texture, suggesting that AsA–GSH pathway may provide important metabolic support for these phenotypic improvements.

Conclusion

The regulatory mechanisms by which DBD plasma treatment maintains postharvest quality of sweet corn. Metabolomics revealed that DBD treatment suppressed the accumulation of deterioration-associated metabolites that progressively accumulated during senescence, while promoting the late-storage recovery of flavor- and nutrition-related metabolites. Transcriptomics revealed that DBD treatment shifted sugar

metabolism from rapid consumption to homeostatic maintenance and intervened in cell wall synthesis and cross-linking, thereby maintaining sweetness and suppressing kernel hardening. Most importantly, the RONS generated by DBD treatment acted as moderate stress signals, triggering the endogenous antioxidant defense system centered on the AsA–GSH cycle. This system coordinately maintained redox homeostasis through the *GST* family, converting exogenous stress into protective responses. These systematic regulations ultimately manifested as quality advantages of greater sugar retention, slower water loss, brighter color, and better texture. This study confirmed the efficacy of DBD treatment in maintaining sweet corn quality and extending storage life, and revealed its molecular mechanisms of senescence delay. To this end, we propose a working model (Fig. 8) that illustrates the mechanisms by which DBD treatment maintains postharvest quality of sweet corn by activating the AsA–GSH-centered antioxidant network and coordinating multiple metabolic pathways.

Materials and Methods

Plant materials and DBD plasma treatment

The sweet corn used in this experiment was the sweet and waxy cultivar 'Nongkenuo 336'. Cobs were harvested from the Xiaotangshan orchard of Beijing Tian'an Agriculture and transported to the laboratory within 2 h of harvest. The husks and silks were removed and the shanks trimmed. Cobs that were uniform in size, free of mechanical damage and pests or diseases, and of uniform maturity were randomly divided into two sets of 60 cobs each. The control cobs (CK) received no treatment, while the DBD cobs were placed in a plasma device for 10 min. The device consisted of a DC high-voltage power supply, a sealed acrylic chamber, a grounded dielectric mesh electrode, a sample-holding mesh

frame, and an anion detector. A metal mesh grounded electrode covered with a dielectric barrier layer was installed at the bottom inside the discharge chamber, while a hollow sample-holding mesh was mounted above it. Fresh sweet corn cobs were laid flat on the surface of the sample-holding mesh. The vertical distance between the sample-holding mesh and the lower grounded dielectric mesh was 9 cm, forming a discharge air gap between the two meshes, and the total height of the chamber was 24 cm. The experiment was performed under constant voltage mode. After applying a DC high voltage of 10.5 kV, the air between the two meshes was broken down under a strong electric field, generating self-triggered microfilament discharge to produce non-thermal plasma. The average discharge current fluctuated in the range of 1.35–1.59 mA under steady-state discharge during treatment. Negative ions and reactive species generated by discharge diffused throughout the chamber and acted on the samples. An anion detector was used to monitor the real-time negative ion concentration inside the sealed chamber. After treatment, both CK and DBD cobs were stored at 20 °C and 90% ± 2% relative humidity. Samples were collected on days 0, 2, 4, 6, and 8 of storage. Both ends of each cob were removed, and the middle section was retained with the kernels kept as intact as possible. The kernels were flash-frozen in liquid nitrogen for physiological measurements and stored at −80 °C until use. Additional samples from days 0 and 8 were used for sequencing.

Determination of firmness, color, soluble solids content (SSC), and weight loss

Firmness was measured with a CTX texture analyzer (Brookfield AMETEK, USA) equipped with a P/2 probe (2 mm diameter). The trigger force, penetration distance, and test speed were set to 10 N, 10.0 mm, and 0.5 mm/s, respectively. Three cobs were randomly selected each time. Three different positions at the maximum transverse diameter

of the middle section of each cob were measured, and the mean value was taken as the firmness each cob.

Color was measured with a CR-400 colorimeter (Konica Minolta, Japan) equipped with a pulsed xenon arc lamp (D65 illuminant equivalent). During measurement, the 8-mm-diameter aperture probe was placed vertically against the kernel surface at the middle section of the cob. Before each measurement, the colorimeter was calibrated with a white standard plate (99% reflectance) (Li et al., 2026). The plate values were L^* = 97.3 ± 0.2, a^* = −0.54 ± 0.01, and b^* = 3.39 ± 0.02. Three cobs were randomly selected each time. Three different positions at the maximum transverse diameter of the middle section of each cob were measured, and the mean value was taken as the kernel color of eachcob.

The SSC was measured with a PAL-1 handheld refractometer (Atago, Guangzhou, China). Three cobs were randomly selected each time. Kernels from three different positions at the maximum transverse diameter of the middle section of each cob were wrapped in clean gauze and squeezed to extract juice. The mean value was taken as the SSC of the kernels of each cob.

Weight loss was determined gravimetrically. Three cobs per group were randomly selected and labeled, then weighed at each storage time point, the mean was used to calculate the weight loss by the difference method.

Metabolite extraction, analysis, and metabolomic data processing

Sample preparation

Each treatment at each sampling time point included three independent biological replicates. After vacuum freeze-drying, 50 mg of sample was weighed and mixed with 1000 μL of extraction solution (methanol: acetonitrile: water = 1:2:1, V/V/V). The mixture

was vortexed for 30 s and ground at 45 Hz for 10 min (Dinghaoyuan grinder). It was then ultrasonicated in an ice-water bath for 10 min and kept at −20 °C for 1 h. Finally, it was centrifuged at 4 °C and 13800 ×g for 15 min. A 300-μL aliquot of the supernatant was filtered through a 0.22-μm organic membrane into a 2-mL injection vial. QC samples were prepared by mixing 10 μL of each sample for instrument analysis. Analysis was performed by ultra-performance liquid chromatography–tandem mass spectrometry (UPLC-MS/MS). The liquid chromatography system was an Acquity I-Class PLUS UPLC (Waters) with an Acquity UPLC HSS T3 column (1.8 μm, 2.1 mm × 100 mm, Waters). The mass spectrometer was a Qtrap 6500+ high-sensitivity mass spectrometer (AB Sciex).

Data analysis

Metabolites were identified based on Q1, Q3, and retention time (RT) using the in-house GB-PLANT database. Quantification was performed in multiple reaction monitoring (MRM) mode on a triple quadrupole mass spectrometer. Peak-area integration was applied to all mass spectral peaks, with integration correction for the same metabolite across samples. Metabolite content data were normalized by unit variance scaling (UV). Heatmaps were drawn with the pheatmap package in R, with hierarchical cluster analysis (HCA) of metabolite accumulation patterns across samples. Identified metabolites were annotated using the KEGG database. Multivariate statistical analyses were performed by partial least squares-discriminant analysis (PLS-DA) and principal component analysis (PCA). Variable importance in projection (VIP) scores were obtained by orthogonal partial least squares-discriminant analysis (OPLS-DA). Differentially accumulated metabolites were screened using fold change ≥ 2, VIP ≥ 1, and $P < 0.05$ as criteria.

RNA extraction, cDNA library construction, sequencing, and transcriptomic data analysis

Sample preparation and library construction

Samples were ground into powder, and three independent biological replicates were prepared for each treatment at each sampling time point. Total RNA was extracted using the RNAprep Pure Plant Kit (Tiangen, Beijing). RNA concentration and purity were determined with a NanoDrop 2000 (Thermo Fisher Scientific, USA). RNA integrity was assessed with an Agilent Bioanalyzer 2100 system (Agilent Technologies, USA) using the RNA Nano 6000 kit. Library construction for each sample started with 1 μg of total RNA, and RNA-seq was performed on the Illumina NovaSeq platform.

Data analysis

Raw data were further processed on the BMKCloud bioinformatics analysis platform (www.biocloud.net). Raw sequencing reads were quality-filtered with Fastp (default parameters), aligned to the reference genome with HISAT2, and assembled per sample with StringTie. Gene expression levels were expressed as FPKM (fragments per kilobase of transcript per million mapped reads). Differential expression analysis was performed with DESeq2, defining differentially expressed genes as those with adjusted $P < 0.01$ and fold change ≥ 2. KEGG pathway enrichment analysis was performed using the KOBAS database and clusterProfiler software.

Protein extraction, LC-MS/MS, and proteomic data analysis

Sample preparation and LC-MS/MS analysis

Corn samples were ground in liquid nitrogen, with three biological replicates each for untreated and treated cob samples for. Sample proteins were extracted with RIPA lysis

buffer and digested with trypsin. The resulting peptides were desalted, vacuum-dried, and resuspended in 0.1% formic acid, and the supernatant was subjected to mass spectrometry. The liquid chromatography system was an Easy-nLC 1200. The mass spectrometer was a Q Exactive HF-X Hybrid Quadrupole-Orbitrap (Thermo Fisher Scientific, USA) equipped with an ESI nano-spray ion source. Astral DIA proteomic analysis was performed in MasterScan and DIA scan modes. Proteomic detection was completed by Qingdao Baipu Biotechnology Co., Ltd.

Data analysis

Raw mass spectrometry data were searched against the species protein database using MaxQuant (1.6.2.10). Parameters were set as follows: fixed modification, carbamidomethylation (C); variable modifications, oxidation (M) and acetyl (Protein N-term); enzyme specificity, trypsin, with a maximum of 2 missed cleavages. Both Precursor Qvalue Cutoff and Protein Qvalue Cutoff were set to 0.01. Protein quantification results were statistically analyzed by t-test. Differential proteins were screened at fold change $\geq$ 1.50 or $\leq$ 1/1.50 and $P \leq 0.05$.

Statistical analysis

Statistical analyses were performed with IBM SPSS Statistics 27 (Two-way ANOVA followed by Sidak's simple effect test was performed. n.s., no significant difference; * $P <$ 0.05, ** $P < 0.01$, *** $P < 0.001$.). Data visualization was completed with CNSknowall, Origin 2021, the Metware Cloud platform (https://cloud.metware.cn/), and Excel. Values represent means ± standard error (n = 3).

Acknowledgments

This research was supported by Beijing Innovation Consortium of Agriculture Research System (BAIC02-2026); the Special Innovation Ability Construction Fund of Beijing Academy of Agricultural and Forestry Sciences (KJCX20261805); and BAAFS Foundation for Excellent Young Scientists (Grant No. YKPY202614).

Data Availability Statement

The datasets generated and/or analyzed during the current study are not publicly available due to the fact that related research is still in progress but are available from the corresponding author on reasonable request.

Competing interest

The authors declare no competing financial or non-financial interests.

Author contributions

Jingjing Jin: Data analysis, Methodology, Validation, Visualization, Data curation, Writing - original draft & editing. Ronghuan Wang, Tianjun Xu: Visualization, Writing - review & editing, Data curation. Christopher B. Watkins: Writing - review & editing. Yunxiang Wang, Yiting Ren: Methodology, Supervision. Hua Chen, Chunmei Bai, Kunyu Sun, Lili Ma, Xuelian He, Zhaorui Li: Methodology, Data curation. Lihong Wang: Conceptualization, Writing - review & editing, Supervision. Jinhua Zuo, Yanyan Zheng: Conceptualization, Writing - review & Editing, Supervision, Funding acquisition, Project administration.

Supplementary information

The following are the Supplementary Material to this article:

Supplementary Material 1. Figures S1-S3

Supplementary Material 2. Tables S1-S6

References

1. Abu Siam, F., Abu-Romman, S., Al-Rubaye, S.A.K., Al-Mohusaien, R.M., Sadder, M.T. *VsAPX1* is up-regulated by ABA and heat stress in common vetch (*Vicia sativa*). Int. J. Plant Biol. **17**, 16(2026).
2. An, F., Chen, T., Zhu, W., Xiao, X., Xue, J., Luo, X., Wei, Z., Li, K., Chen, S., Cai, J. Systematic analysis of cinnamyl alcohol dehydrogenase family in cassava and validation of *MeCAD13* and *MeCAD28* in lignin synthesis and postharvest physiological deterioration. Int. J. Mol. Sci. **25**, 11668(2024).
3. Bai, B., van der Horst, N., Cordewener, J.H., America, A.H.P., Nijveen, H., Bentsink, L. Delayed protein changes during seed germination. Front Plant SCI. **12**,735719(2021).
4. Becerra-Sanchez, F., Taylor, G. Reducing post-harvest losses and improving quality in sweet corn (*Zea mays* L.): challenges and solutions for less food waste and improved food security. Food Energy Secur. **10**, e277(2021).
5. Chen, H., Zuo, J., Wang, Y., Li, T., Bai, C., Alisdair R., Wang, R., Shi, Y., Tao, J., Feng, X., Ren, Y., Wang, L., Zheng, Y. Effects of low-voltage electrostatic field on post-harvest sugar metabolism and stress resistance in sweet corn. Postharvest Biol. Technol. **231**, 113859(2026a).
6. Chen, H., Wang, L., Wang, Y., Jing, Z., Wang, R., Shi, Y., Bai, C., Ma, L., Liu, S., Zuo, J., Zheng, Y. Microwave effects on the flavor and storage quality of 'Nongke Nuo 336' sweet corn. J. Future Foods. **7**, 778-792(2027).

7. Chen, J., Liang, C., He, X., Huang, J., Huang, W., Huang, A., Yang, Y., Hong, G., Chen, Y., Zeng, D., Guo, J., He, Y. Advances in the function roles of hydroxycinnamoyl-CoA shikimate/quinate hydroxycinnamoyl transferases: a key enzyme linking phenylpropanoid metabolism to plant terrestrial adaptation. Plants. **15**, 1162(2026b).
8. Chen, S., Zheng, Y., Fan, W., Bai, C., Ma, L., Zhou, X., Wang, R., Shi, Y., Cai, W., Wang, Q., Watkins, C.B., Zuo, J. Unravelling the postharvest quality diversities of different sweet corn varieties. Postharvest Biol. Technol. **209**, 112718(2024).
9. Lecourieux, F., et al. Proteomic and metabolomic profiling underlines the stage- and time-dependent effects of high temperature on grape berry metabolism. J. Integr. Plant Biol. **62**, 1132-1158(2020).
10. Decros, G., Baldet, P., Beauvoit, B., Stevens, R., Flandin, A., Colombié, S., Gibon, Y., Pétriacq, P. Get the balance right: ROS homeostasis and redox signalling in fruit. Front. Plant Sci. **10**,1091(2019).
11. Eh, T.J., Jiang, Y., Jiang, M., Li, J., Lei, P., Ji, X., Kim, H.I., Zhao, X., Meng, F. The role of trehalose metabolism in plant stress tolerance. J. Adv. Res. **76**, 57-72(2025).
12. Engel, J., Schmalhorst, P.S., Routier, F.H. Biosynthesis of the fungal cell wall polysaccharide galactomannan requires intraluminal GDP-mannose. J. Biol. Chem. **287**, 44418-44424(2012).
13. He, X., Sun, T., Zhang, W., Yang, W., Li, L., Cao, J., Guo, M., Chen, G. Cold plasma treatment maintains antioxidant capacity and cell membrane integrity in apricot fruit by inducing reactive oxygen species scavenging systems. Postharvest Biol. Technol. **230**, 113815(2025a).

14. He, X., Zhang, W., Sun, T., Yang, W., Li, L., Guo, M., Chen, G. Cold plasma treatment maintains apricot fruit quality by regulating respiration and energy metabolism. LWT. **227**, 117991(2025b).
15. Huang, Q., Huang, L., Chen, J., Zhang, Y., Kai, W., Chen, C. Maintenance of postharvest storability and overall quality of 'Jinshayou' pummelo fruit by salicylic acid treatment. Front Plant SCI. **13**, 1086375(2023a).
16. Huang, W., Shi, Y., Yan, H., Wang, H., Wu, D., Grierson, D., Chen, K. The calcium-mediated homogalacturonan pectin complexation in cell walls contributes the firmness increase in loquat fruit during postharvest storage. J. Adv. Res. **49**, 47-62(2023b).
17. Ifigeneia, M., Koukounaras, A., Kostas, S., Patelou, E., Kanellis, A. Regulation of vitamin C accumulation for improved tomato fruit quality and alleviation of abiotic stress. Genes. **12**, 694(2021).
18. Jia, S., Zhang, N., Ji, H., Zhang, X., Dong, C., Yu, J., Yan, S., Chen, C., Liang, L., 2022. Effects of atmospheric cold plasma treatment on the storage quality and chlorophyll metabolism of postharvest tomato. Foods. **11**, 4088(2022).
19. Li, K., Zeng, J., Zhang, N., Yu, Y., Zhu, W., Li, G., Hu, J. Multi-layer molecular analysis reveals distinctive metabolomic and transcriptomic profiles of different sweet corn varieties. Front. Plant Sci. **15**, 1453031(2024).
20. Li, T., Wang, Z., Wang, Y., Watkins, C.B., Chen, H., Bai, C., Tao, J., Ma, L., Wang, R., Shi, Y., Feng, X., Liu, S., Zuo, J., Zheng, Y. Ozone treatment maintains the sweetness and volatile odor of sweet corn by enhancing antioxidant capacity and resistance to disease. Postharvest Biol. Technol. **231**, 113947(2026).

21. Li, Y., Fan, K., Shen, J., Wang, Y., Jeyaraj, A., Hu, S., Chen, X., Ding, Z., Li, X. Glycine-induced phosphorylation plays a pivotal role in energy metabolism in roots and amino acid metabolism in leaves of tea plant. Foods. **12**, 334(2023).
22. Linster, C.L., Clarke, S.G. L-ascorbate biosynthesis in higher plants: the role of VTC2. Trends Plant Sci. **13**, 567-573(2008).
23. Liu, H., Li, D., Xu, W., Fu, Y., Liao, R., Shi, J., Chen, Y. Application of passive modified atmosphere packaging in the preservation of sweet corns at ambient temperature. LWT. **136**, 110295(2021).
24. Liu, M., Wang, C., Ji, H., Sun, M., Liu, T., Wang, J., Cao, H., Zhu, Q. Ethylene biosynthesis and signal transduction during ripening and softening in non-climacteric fruits: an overview. Front. Plant Sci. **15**, 1368692(2024a).
25. Liu, S., Zheng, Y., Wang, R., Shi, Y., Cai, W., Xu, T., Wu, C., Ma, L., Bai, C., Zhou, X., Wang, Q., Watkins, C.B., Zuo, J., 2024b. Chlorine dioxide affects metabolism of harvested sweet corn. Postharvest Biol. Technol. **211**, 112834(2024b).
26. Liu, Y., Fan, R., Chen, L., Pei, J., Deng, Y., Dong, K., Wang, L. Unveiling the role of *VcCOMT38* as a specific O-methyltransferase for enhancing lignin biosynthesis: insights from blueberry and cross-species analysis. Hortic. Plant J. **12**, 85-98(2026).
27. Ma, L., Wang, Y., Ren, Y., Wu, C., Jiang, Y., Tao, J., He, X., Feng, X., Li, T., Liu, X., Jin, J., Zuo, J., Zheng, Y. FVRS: a cross-species multi-omics database for fruit and vegetable ripening and senescence. Mol. Hortic. **6**, 79(2026).
28. Mehravi, S., Hanifei, M., Sohrabi, S.S., Khodadadi, M., Gholizadeh, A. Exploring metabolite profiles and phenylpropanoids biosynthesis gene expression in *Pimpinella anisum* L. under water deficit stress. BMC Plant Biol. **25**, 1722(2025).

29. Mushtaq, A., Jabeen, A., Yousouf, M., Malik, M.A., Mukhtar, T., Amin, T., Showkat, S., Rafiq, A. Post-harvest quality management of sweet corn: disorders, losses and preservation strategies. Food Nutr. **1**, 100007(2025).
30. Nikzadfar, M., Kazemi, A., Abooei, R., Abbaszadeh, R., Firouz, M.S., Akbarnia, A., Rashvand, M. Application of cold plasma technology on the postharvest preservation of in-packaged fresh fruit and vegetables: recent challenges and development. Food Bioprocess Technol. **17**, 4473-4505(2024).
31. Nishizawa, A., Yabuta, Y., Shigeoka, S. Galactinol and raffinose constitute a novel function to protect plants from oxidative damage. Plant Physiol. **147**, 1251-1263(2008).
32. Okuyama, M., Saburi, W., Mori, H., Kimura, A. α-Glucosidases and α-1,4-glucan lyases: structures, functions, and physiological actions. Cell. Mol. Life Sci. **73**, 2727-2751(2016).
33. Pizzio, G.A. The role of abscisic acid (ABA) machinery in stress response. Plants. **14**, 935(2025).
34. Ren, M., Wang, M., Wang, D., Huang, Y., Du, L. Identification of candidate gene controlling soluble sugar degradation during postharvest storage of sweet corn based on BSA-seq. Genes. **17**, 291(2026).
35. Romero, P., Lafuente, M.T., Rodrigo, M.J. The *citrus* ABA signalosome: identification and transcriptional regulation during sweet orange fruit ripening and leaf dehydration. J. Exp. Bot. **63**, 4931-4945(2012).

995 36. Shi, L., Chen, Y., Dong, W., Li, S., Chen, W., Yang, Z., Cao, S. Melatonin delayed
996 senescence by modulating the contents of plant signalling molecules in postharvest
997 okras. Front. Plant Sci. **15**, 1304913(2024).
998 37. Shishir, M.R.I., Kamal, M.M., Karim, N., Saifullah, M., Khan, S., Zhang, K.,
999 Marappan, G., Aalim, H., Hashim, S.B.H., Zhai, X., Liu, Z., Tahir, H.E., Taip, F.S.,
1000 Zou, X. Cold plasma and integrated approaches for fresh produce preservation:
1001 mechanisms, quality attributes, challenges, and future directions. Trends Food Sci.
1002 Technol. **159**, 104988(2025).
1003 38. Singh, S.P., Thakur, R. Postharvest applications of cold plasma treatment for
1004 improving food safety and sustainability outcomes for fresh horticultural produce.
1005 Postharvest Biol. Technol. **209**, 112694(2024).
1006 39. Storch, T.T., Pegoraro, C., Quecini, V., Rombaldi, C.V., Girardi, C.L. Novel targets for
1007 fruit conservation strategies revealed by omics studies: a systematic review and meta-
1008 analysis. Int. J. Food Sci. **2025**, 9963581(2025).
1009 40. Subrahmanyam, K., Gul, K., Sehrawat, R., Allai, F.M. Impact of in-package cold
1010 plasma treatment on the physicochemical properties and shelf life of button
1011 mushrooms (*Agaricus bisporus*). Food Biosci. **52**, 102425(2023).
1012 41. Tahir, H., Sajjad, M., Qian, M., Zeeshan Ul Haq, M., Tahir, A., Farooq, M.A., Wei, L.,
1013 Shi, S., Zhou, K., Yao, Q. Glutathione and ascorbic acid accumulation in mango pulp
1014 under enhanced UV-B based on transcriptome. Antioxidants. **13**, 1429(2024).
1015 42. Tang, N., Cao, Z., Yang, C., Ran, D., Wu, P., Gao, H., He, N., Liu, G., Chen, Z. A
1016 R2R3-MYB transcriptional activator LmMYB15 regulates chlorogenic acid

biosynthesis and phenylpropanoid metabolism in Lonicera macranthoides. Plant Sci. **308**, 110924(2021).

43. Tappi, S., Ragni, L., Tylewicz, U., Romani, S., Ramazzina, I., Rocculi, P. Browning response of fresh-cut apples of different cultivars to cold gas plasma treatment. Innov. Food Sci. Emerg. Technol. **53**, 56-62(2019).
44. Teng, Y., Ou, M., Wu, J., Jiang, T., Zheng, K., Guo, Y., Pan, D., Zhang, T., Wu, Z. Emulsifying properties of oat protein/casein complex prepared using atmospheric cold plasma with pH shifting. Foods. **14**, 2702(2025).
45. Wang, C., Liu, H., Liu, C., Wei, Y., Wang, J., Zhang, Y., Wang, X., Chen, B., Yan, W., Qiao, Y. Effects of slightly acidic electrolyzed water on the quality and antioxidant capacity of fresh red waxy corn during postharvest cold storage. Front. Plant Sci. **15**, 1428394(2024a).
46. Wang, C., Meng, L., Zhang, G., Yang, X., Pang, B., Cheng, J., He, B., Sun, F. Unraveling crop enzymatic browning through integrated omics. Front. Plant Sci. **15**, 1342639(2024b).
47. Wang, D., Zhao, X., Su, T., Wang, W., Xin, X., Zhang, B., Zhang, D., Yu, Y., Wang, Z., Zhang, F., Zhou, L., Li, P., Yu, S. Exogenous gibberellin delays postharvest leaf senescence in pak choi by modulating transcriptomic and metabolomic profiles. Foods, **14**, 981(2025).
48. Warinowski, T., Koutaniemi, S., Kärkönen, A., Sundberg, I., Toikka, M., Simola, L.K., Kilpeläinen, I., Teeri, T.H. Peroxidases bound to the growing lignin polymer produce natural like extracellular lignin in a cell culture of Norway spruce. Front. Plant Sci. **7**, 1523(2016).

49. Wu, Z., Fan, G., Wu, C., Li, T., Zhou, D., Li, X., Yan, Z., Cong, K., Hua, X. Dielectric barrier discharge plasma delayed the textural hardening of bamboo shoots by regulating cell wall metabolism. Scientia Hortic. **321**, 112322(2023).
50. Xiao, J., Cao, B.Y., Tang, W., Sui, X., Tang, Y., Lai, Y., Sun, B., Huang, Z., Zheng, Y.-D., Li, H.X. The CaCAD1-CaPOA1 module positively regulates pepper resistance to cold stress by increasing lignin accumulation. Int. J. Biol. Macromol. **290**, 139979(2025).
51. Xiao, Y., Xie, L., Li, Y., Li, C., Yu, Y., Hu, J., Li, G. Impact of low temperature on the chemical profile of sweet corn kernels during post-harvest storage. Food Chem. **431**, 137079(2024).
52. Xu, L., Gao, Z., Li, L., Guo, J. Impact of dielectric barrier discharge cold plasma on anthocyanin metabolism in blueberries: a targeted metabonomic and transcriptomic analysis. Postharvest Biol. Technol. **213**, 112963(2024).
53. Yan, B., Wang, Y., Bai, Y., Liu, Z., Liu, H., Chen, X., Shen, Y., Duan, L. Insights into the senescent mechanisms of harvested strawberry fruit at the physiological, molecular and metabolic levels. Fruit Res. **4**, e018(2024).
54. Zhang, C., Cheng, J.-H. Assessing the effect of cold plasma on the softening of postharvest blueberries through reactive oxygen species metabolism using transcriptomic analysis. Foods. **13**, 1132(2024).
55. Zhang, J., Wang, C., Zhang, M., Pu, Y., Xiang, Y. Effects of different packaging methods on the quality of fresh red apricots during simulated transportation and storage after transportation. Foods. **15**, 2068(2026).

56. Zhang, S., Song, X., Qin, Y. Characterization of UDP-glucose pyrophosphorylases from different organisms. Biosci. Rep. **45**, 263-276(2025a).
57. Zhang, X., Zhang, W., Liu, Y., Yang, W., Cao, J., Guo, M., Chen, G. Spermidine treatment delays postharvest senescence of prune (*Prunus domestica* L.) fruit by regulating reactive oxygen species and membrane lipid metabolism. Postharvest Biol. Technol. **228**, 113670(2025b).
58. Zhang, Y.-J., Huang, Q., Li, A.-R., Gan, Z.-Y., Zeng, J., Kai, W.-B., Chen, C., Chen, J.-Y. Apple polyphenols delay postharvest senescence and quality deterioration of 'Jinshayou' pummelo fruit during storage. Front. Plant Sci. **13**, 1117106(2023).
59. Zhao, Y., Shi, W., Wang, Z., Yan, Z., Shi, J., Zuo, J., Feng, B., Wang, Q. Integrated analysis of transcriptomic and metabolomic data reveals how slurry ice treatment affects sugar metabolism in sweet corn (*Zea mays* L. var. *saccharata*) during cold storage. Food Front. **5**, 1722-1736(2024).
60. Ziuzina, D., Misra, N.N., Han, L., Cullen, P.J., Moiseev, T., Mosnier, J.P., Keener, K., Gaston, E., Vilaró, I., Bourke, P. Investigation of a large gap cold plasma reactor for continuous in-package decontamination of fresh strawberries and spinach. Innov. Food Sci. Emerg. Technol. **59**, 102229(2020).

Figures

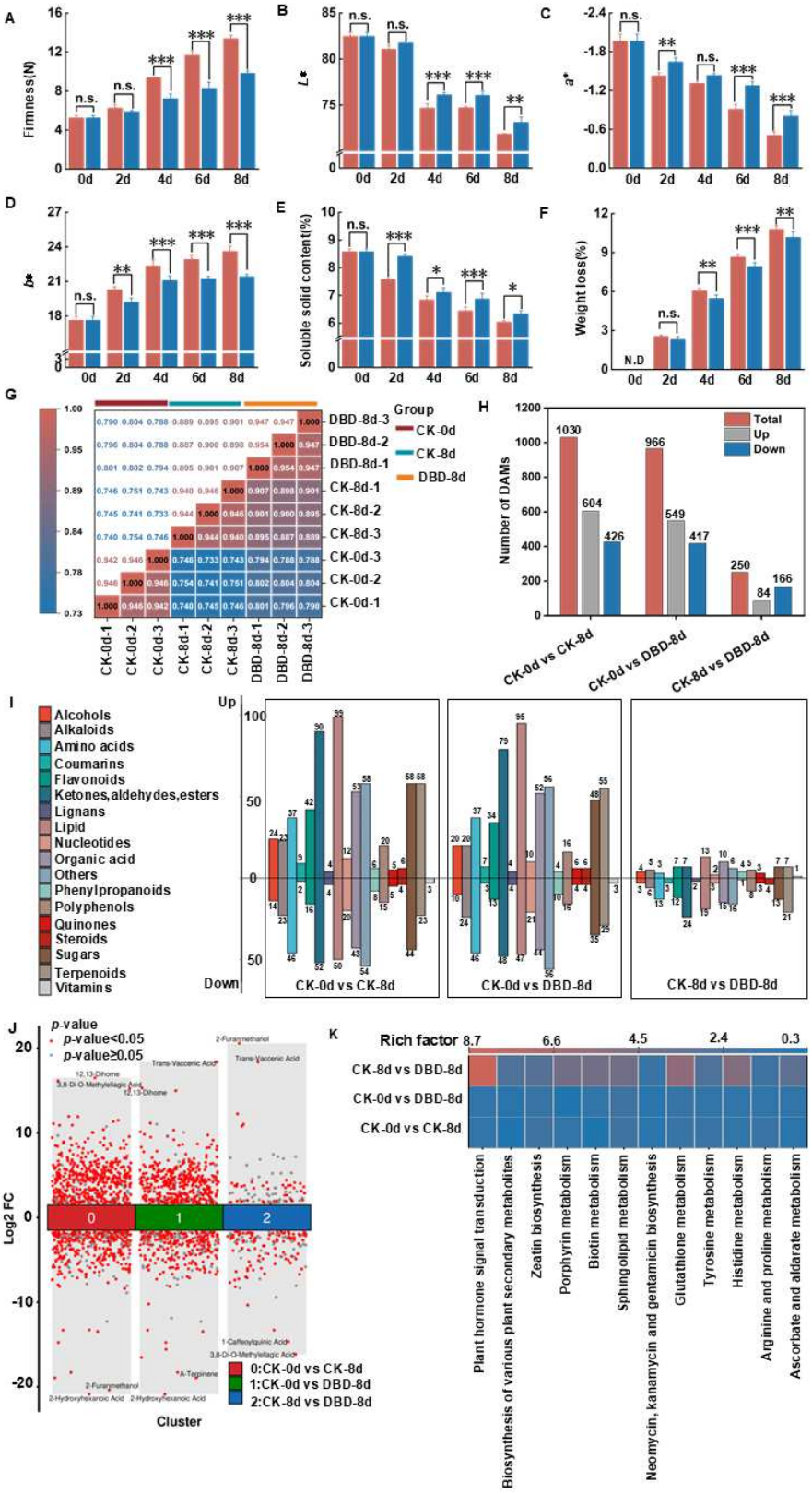
A
Firmness(N)
B
L*
C
a*
D
b*
E
Soluble solid content(%)
F
Weight loss(%)
N.D
0d
2d
4d
6d
8d
n.s.
G
Group
CK-0d
CK-8d
DBD-8d
DBD-8d-3
DBD-8d-2
DBD-8d-1
CK-8d-1
CK-8d-2
CK-8d-3
CK-0d-3
CK-0d-2
CK-0d-1
H
Number of DAMs
Total
Up
Down
1030
604
426
966
549
417
250
84
166
CK-0d vs CK-8d
CK-0d vs DBD-8d
CK-8d vs DBD-8d
I
Alcohols
Alkaloids
Amino acids
Coumarins
Flavonoids
Ketones,aldehydes,esters
Lignans
Lipid
Nucleotides
Organic acid
Others
Phenylpropanoids
Polyphenols
Quinones
Steroids
Sugars
Terpenoids
Vitamins
Up
Down
J
p-value
p-value<0.05
p-value≥0.05
Log2 FC
Cluster
0:CK-0d vs CK-8d
1:CK-0d vs DBD-8d
2:CK-8d vs DBD-8d
K
Rich factor
8.7
6.6
4.5
2.4
0.3
CK-8d vs DBD-8d
CK-0d vs DBD-8d
CK-0d vs CK-8d
Plant hormone signal transduction
Biosynthesis of various plant secondary metabolites
Zeatin biosynthesis
Porphyrin metabolism
Biotin metabolism
Sphingolipid metabolism
Neomycin, kanamycin and gentamicin biosynthesis
Glutathione metabolism
Tyrosine metabolism
Histidine metabolism
Arginine and proline metabolism
Ascorbate and aldarate metabolism

Fig. 1. Physicochemical quality and metabolomic profiling of sweet corn under CK and DBD plasma treatment during postharvest storage: Firmness (A), *L** value (B), *a** value (C), *b** value (D), soluble solids content (SSC) (E), weight loss (F), correlation heatmap of metabolomic biological replicates (G), statistics of differentially accumulated metabolites (DAMs) in three comparative groups (H), classification overview of DAMs (I), representative differential metabolite abundance profiles (J), shared KEGG enrichment pathways across three comparisons (K) for CK and DBD-treated sweet corn. (A) Fruit firmness during storage. Values represent means ± standard error (n = 3). Two-way ANOVA followed by Sidak's simple effect test was performed. n.s., no significant difference; * $P < 0.05$, ** $P < 0.01$, *** $P < 0.001$.

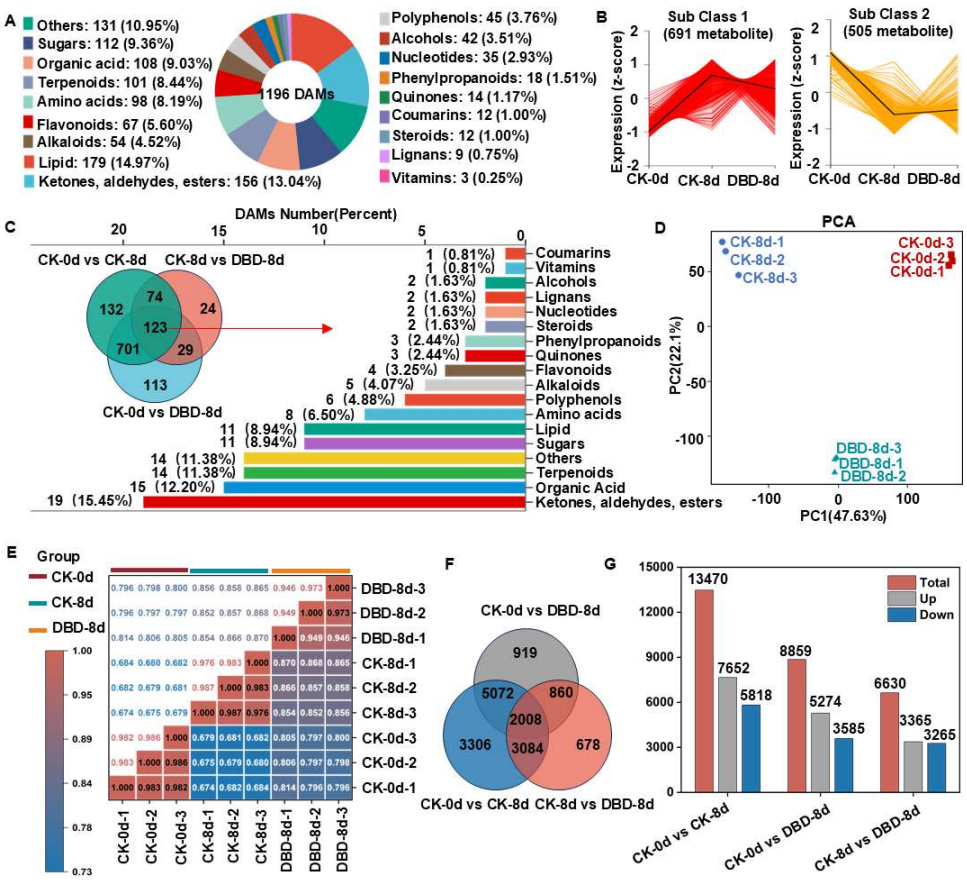

Fig. 2. Global metabolomic and transcriptomic overview of sweet corn responding to DBD plasma treatment: Summary of total detected DAMs (A), K-means clustering of 1196 DAMs showing two major accumulation subclasses (B), Venn diagram of DAMs from three comparative groups (C), PCA plot of transcriptome samples (D), Pearson correlation heatmap for transcriptomic biological replicates (E), Venn diagram of differentially expressed genes (DEGs) from three comparative groups (F), statistics of up- and down-regulated DEGs in each comparison (G) for CK and DBD-treated sweet corn.

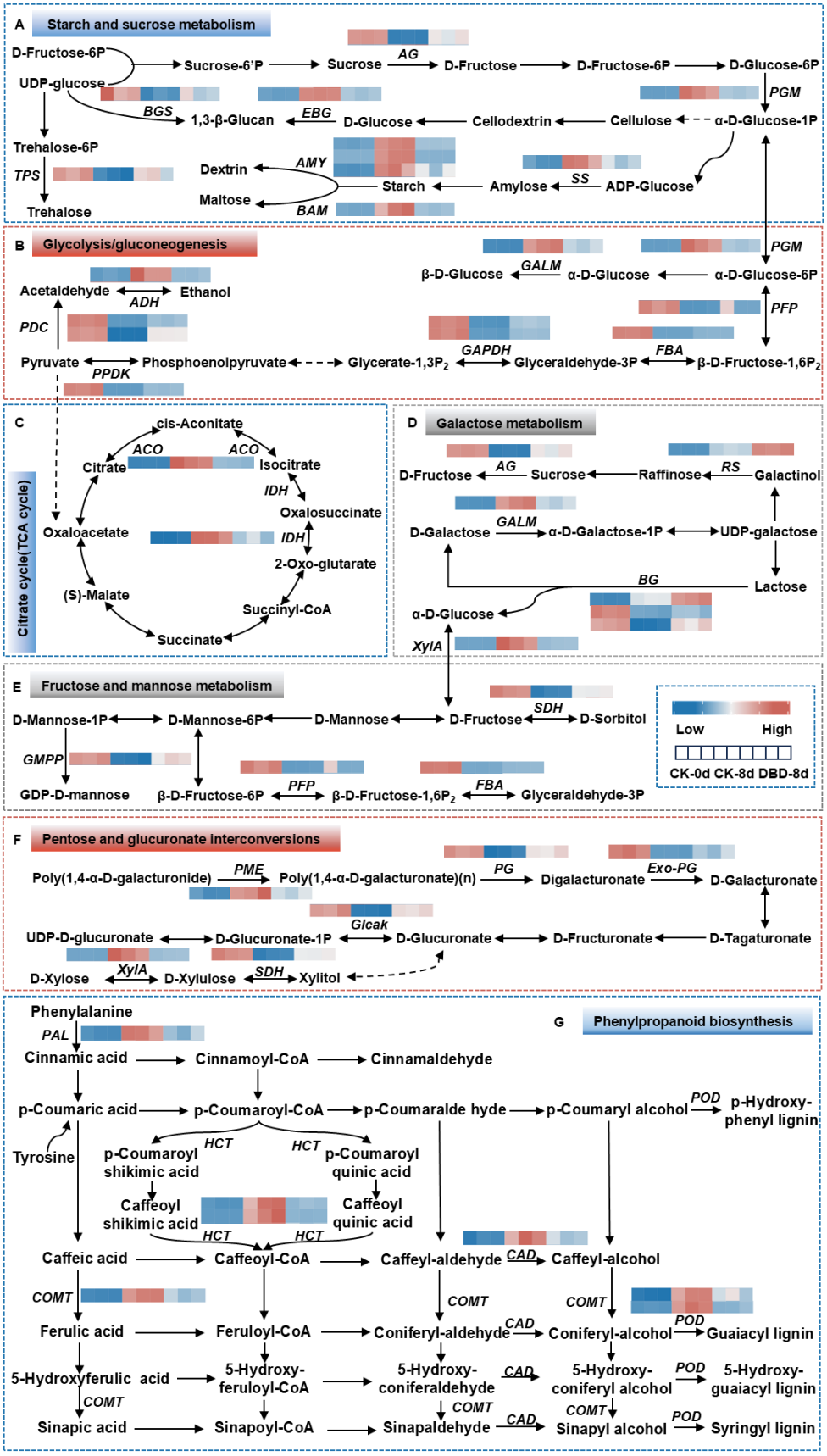
A
Starch and sucrose metabolism
D-Fructose-6P
Sucrose-6'P
Sucrose
AG
D-Fructose
D-Fructose-6P
D-Glucose-6P
UDP-glucose
PGM
BGS
1,3-β-Glucan
EBG
D-Glucose
Cellodextrin
Cellulose
α-D-Glucose-1P
Trehalose-6P
TPS
Trehalose
Dextrin
AMY
Starch
Maltose
BAM
Amylose
SS
ADP-Glucose
B
Glycolysis/gluconeogenesis
PGM
β-D-Glucose
GALM
α-D-Glucose
α-D-Glucose-6P
Acetaldehyde
ADH
Ethanol
PFP
PDC
GAPDH
FBA
Pyruvate
Phosphoenolpyruvate
Glycerate-1,3P2
Glyceraldehyde-3P
β-D-Fructose-1,6P2
PPDK
C
Citrate cycle(TCA cycle)
cis-Aconitate
ACO
ACO
Citrate
Isocitrate
IDH
Oxalosuccinate
Oxaloacetate
IDH
2-Oxo-glutarate
(S)-Malate
Succinyl-CoA
Succinate
D
Galactose metabolism
D-Fructose
AG
Sucrose
Raffinose
RS
Galactinol
D-Galactose
GALM
α-D-Galactose-1P
UDP-galactose
BG
Lactose
α-D-Glucose
XylA
E
Fructose and mannose metabolism
D-Mannose-1P
D-Mannose-6P
D-Mannose
D-Fructose
SDH
D-Sorbitol
GMPP
GDP-D-mannose
β-D-Fructose-6P
PFP
β-D-Fructose-1,6P2
FBA
Glyceraldehyde-3P
Low
High
CK-0d CK-8d DBD-8d
F
Pentose and glucuronate interconversions
Poly(1,4-α-D-galacturonide)
PME
Poly(1,4-α-D-galacturonate)(n)
PG
Digalacturonate
Exo-PG
D-Galacturonate
Glcak
UDP-D-glucuronate
D-Glucuronate-1P
D-Glucuronate
D-Fructuronate
D-Tagaturonate
XylA
SDH
D-Xylose
D-Xylulose
Xylitol
G
Phenylpropanoid biosynthesis
Phenylalanine
PAL
Cinnamic acid
Cinnamoyl-CoA
Cinnamaldehyde
p-Coumaric acid
p-Coumaroyl-CoA
p-Coumaralde hyde
p-Coumaryl alcohol
POD
p-Hydroxy-phenyl lignin
Tyrosine
HCT
HCT
p-Coumaroyl shikimic acid
p-Coumaroyl quinic acid
Caffeoyl shikimic acid
Caffeoyl quinic acid
HCT
HCT
Caffeic acid
Caffeoyl-CoA
Caffeyl-aldehyde
CAD
Caffeyl-alcohol
COMT
COMT
COMT
Ferulic acid
Feruloyl-CoA
Coniferyl-aldehyde
CAD
Coniferyl-alcohol
POD
Guaiacyl lignin
5-Hydroxyferulic acid
5-Hydroxy-feruloyl-CoA
5-Hydroxy-coniferaldehyde
CAD
5-Hydroxy-coniferyl alcohol
POD
5-Hydroxy-guaiacyl lignin
COMT
COMT
COMT
Sinapic acid
Sinapoyl-CoA
Sinapaldehyde
CAD
Sinapyl alcohol
POD
Syringyl lignin

1099

Fig. 3. Transcriptomic changes in carbohydrate, energy and cell-wall-related KEGG pathways induced by DBD plasma treatment. KEGG pathway diagrams show gene heatmaps based on FPKM values after row-wise Z-score transformation. A blue-to-red gradient represents low to high relative gene expression. Expression profiles of key genes in starch-sucrose metabolism (A), glycolysis/gluconeogenesis (B), TCA cycle (C), galactose metabolism (D), fructose and mannose metabolism (E), pentose and glucuronate interconversions (F), phenylpropanoid biosynthesis pathway (G) for CK and DBD-treated sweet corn.

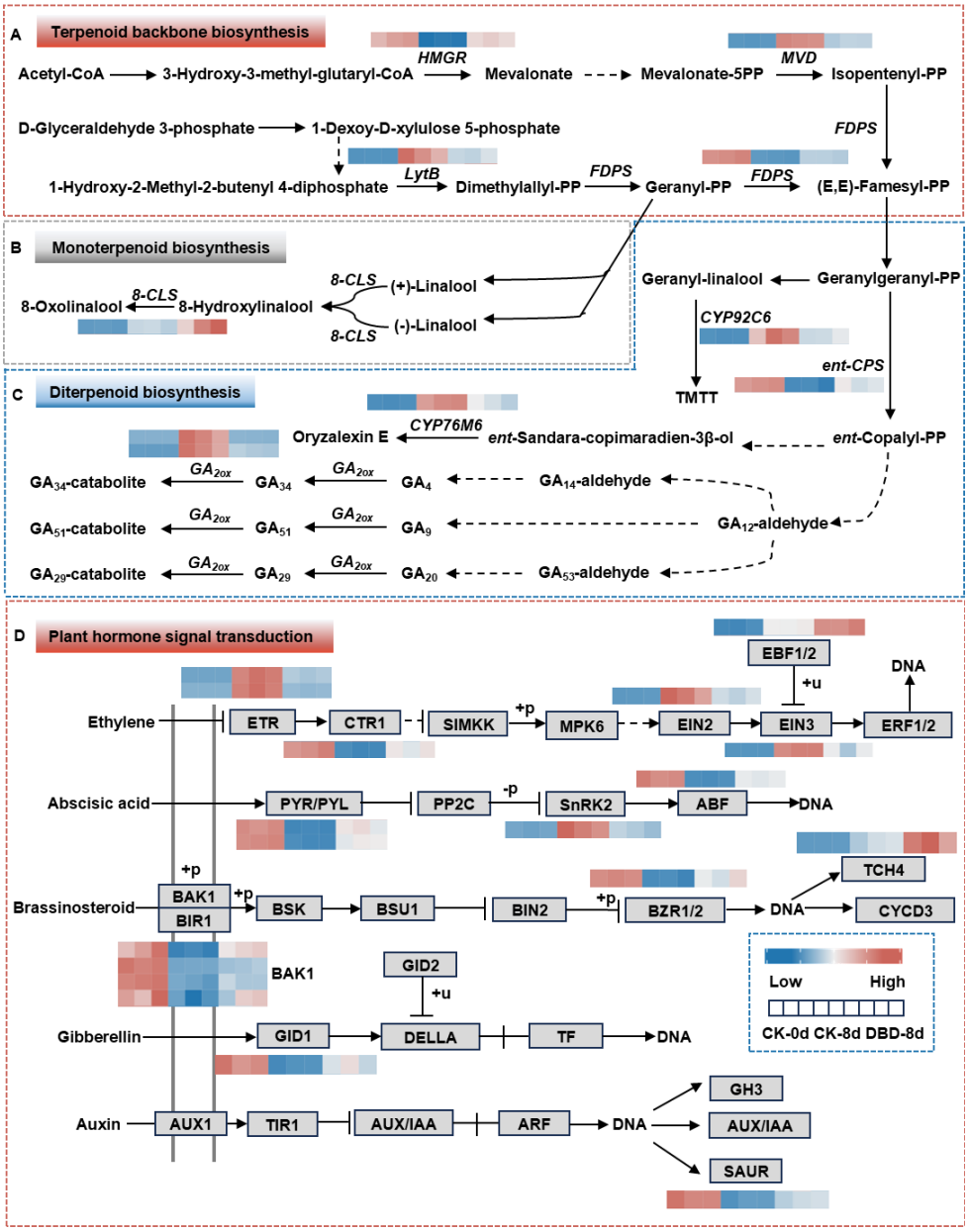
A
Terpenoid backbone biosynthesis
Acetyl-CoA
3-Hydroxy-3-methyl-glutaryl-CoA
HMGR
Mevalonate
Mevalonate-5PP
MVD
Isopentenyl-PP
D-Glyceraldehyde 3-phosphate
1-Dexoy-D-xylulose 5-phosphate
FDPS
1-Hydroxy-2-Methyl-2-butenyl 4-diphosphate
LytB
Dimethylallyl-PP
FDPS
Geranyl-PP
FDPS
(E,E)-Famesyl-PP
B
Monoterpenoid biosynthesis
8-Oxolinalool
8-CLS
8-Hydroxylinalool
8-CLS
(+)-Linalool
8-CLS
(-)-Linalool
Geranyl-linalool
Geranylgeranyl-PP
CYP92C6
TMTT
ent-CPS
C
Diterpenoid biosynthesis
Oryzalexin E
CYP76M6
ent-Sandara-copimaradien-3β-ol
ent-Copalyl-PP
GA34-catabolite
GA20ox
GA34
GA20ox
GA4
GA14-aldehyde
GA51-catabolite
GA20ox
GA51
GA20ox
GA9
GA12-aldehyde
GA29-catabolite
GA20ox
GA29
GA20ox
GA20
GA53-aldehyde
D
Plant hormone signal transduction
EBF1/2
+u
DNA
Ethylene
ETR
CTR1
SIMKK
+p
MPK6
EIN2
EIN3
ERF1/2
Abscisic acid
PYR/PYL
PP2C
-p
SnRK2
ABF
DNA
+p
TCH4
Brassinosteroid
BAK1
BIR1
+p
BSK
BSU1
BIN2
+p
BZR1/2
DNA
CYCD3
BAK1
GID2
+u
Low
High
CK-0d CK-8d DBD-8d
Gibberellin
GID1
DELLA
TF
DNA
GH3
Auxin
AUX1
TIR1
AUX/IAA
ARF
DNA
AUX/IAA
SAUR

1108

Fig. 4. Transcriptomic responses of secondary metabolism and plant hormone signal transduction to DBD plasma treatment. KEGG pathway diagrams show gene heatmaps based on FPKM values after row-wise Z-score transformation. A blue-to-red gradient represents low to high relative gene expression. Gene expression heatmap for terpenoid backbone biosynthesis (A), monoterpene biosynthesis (B), diterpene biosynthesis (C), schematic overview and key DEG expression of plant hormone signal transduction pathways (D) for CK and DBD-treated sweet corn.

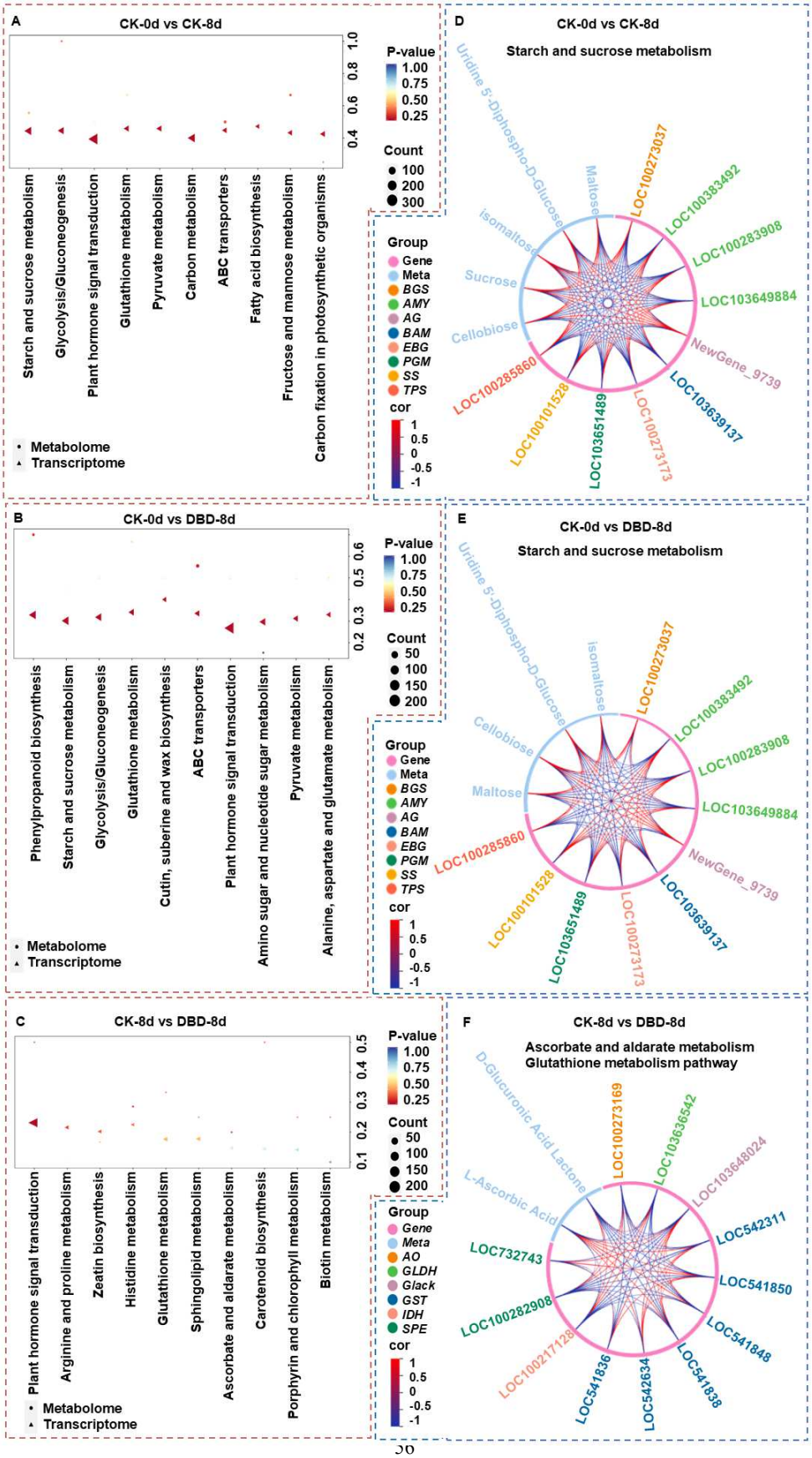
A
CK-0d vs CK-8d
Starch and sucrose metabolism
Glycolysis/Gluconeogenesis
Plant hormone signal transduction
Glutathione metabolism
Pyruvate metabolism
Carbon metabolism
ABC transporters
Fatty acid biosynthesis
Fructose and mannose metabolism
Carbon fixation in photosynthetic organisms
P-value
Count
Group
Gene
Meta
BGS
AMY
AG
BAM
EBG
PGM
SS
TPS
cor
Metabolome
Transcriptome
D
CK-0d vs CK-8d
Starch and sucrose metabolism
Uridine 5'-Diphospho-D-Glucose
Maltose
isomaltose
Sucrose
Cellobiose
LOC100273037
LOC100383492
LOC100283908
LOC103649884
NewGene_9739
LOC103639137
LOC100273173
LOC103651489
LOC100101528
LOC100285860
B
CK-0d vs DBD-8d
Phenylpropanoid biosynthesis
Starch and sucrose metabolism
Glycolysis/Gluconeogenesis
Glutathione metabolism
Cutin, suberine and wax biosynthesis
ABC transporters
Plant hormone signal transduction
Amino sugar and nucleotide sugar metabolism
Pyruvate metabolism
Alanine, aspartate and glutamate metabolism
E
CK-0d vs DBD-8d
Starch and sucrose metabolism
C
CK-8d vs DBD-8d
Plant hormone signal transduction
Arginine and proline metabolism
Zeatin biosynthesis
Histidine metabolism
Glutathione metabolism
Sphingolipid metabolism
Ascorbate and aldarate metabolism
Carotenoid biosynthesis
Porphyrin and chlorophyll metabolism
Biotin metabolism
F
CK-8d vs DBD-8d
Ascorbate and aldarate metabolism
Glutathione metabolism pathway
D-Glucuronic Acid Lactone
L-Ascorbic Acid
LOC100273169
LOC103636542
LOC103648024
LOC542311
LOC541850
LOC541848
LOC541838
LOC542634
LOC541836
LOC100217128
LOC100282908
LOC732743

Fig. 5. Integrated transcriptome-metabolome correlation analysis of sweet corn under DBD plasma treatment. In bubble plots (A-C), bubble size represents the count of enriched genes or metabolites, and bubble color gradient from blue to red corresponds to low-to-high significance of KEGG enrichment. circle nodes represent metabolites, triangle nodes represent genes. In correlation networks (D-F), red lines indicate positive correlation and blue lines indicate negative correlation; Bubble plots of top-10 KEGG enrichment for three comparative groups (A-C), correlation network between DEGs and DAMs in starch-sucrose metabolism for CK-0d vs CK-8d (D), correlation network between DEGs and DAMs in starch-sucrose metabolism for CK-0d vs DBD-8d (E), correlation network between DEGs and DAMs in AsA-GSH antioxidant pathway for CK-8d and DBD-8d (F).

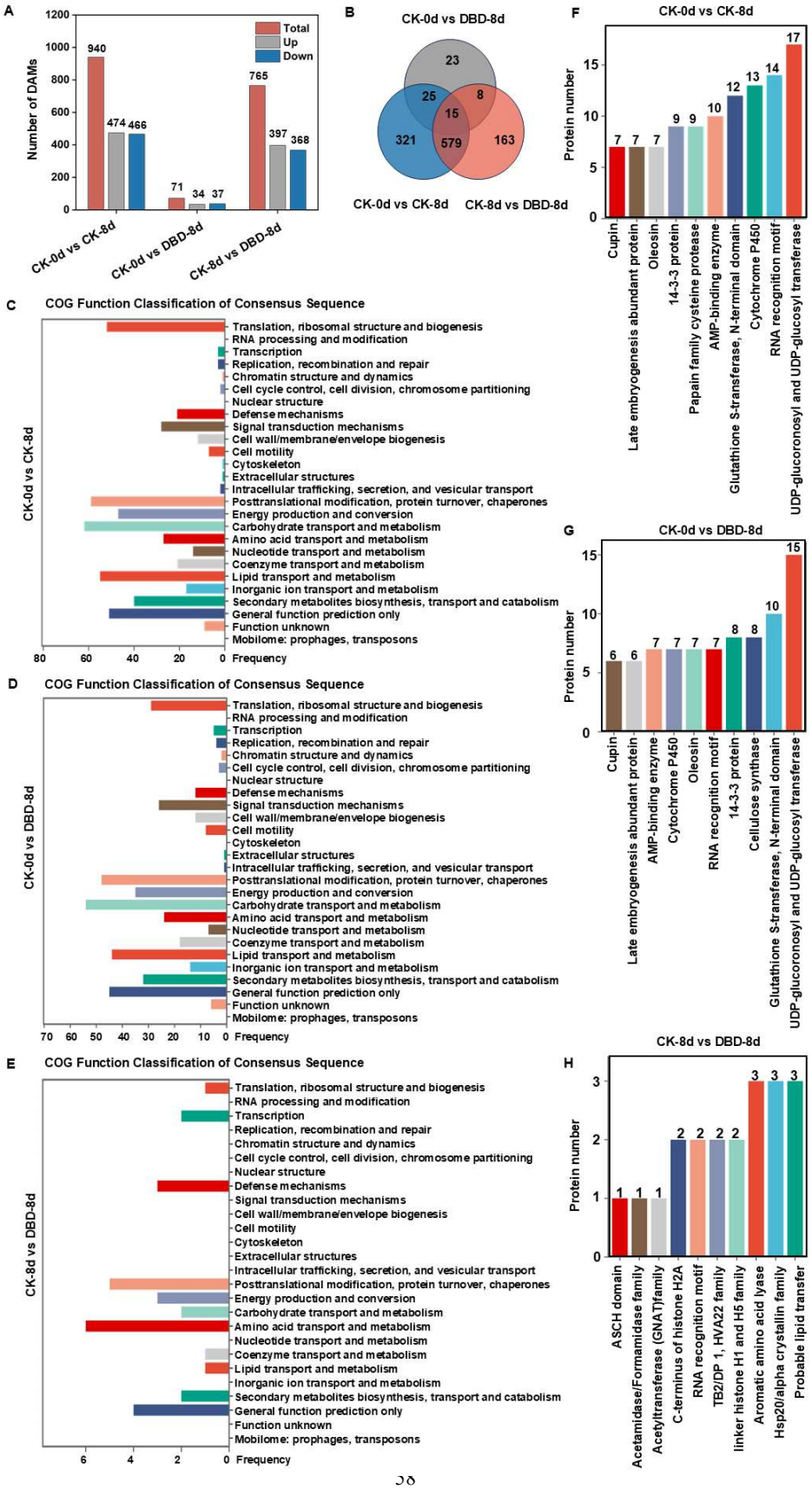
A
Number of DAMs
Total
Up
Down
940
474
466
71
34
37
765
397
368
CK-0d vs CK-8d
CK-0d vs DBD-8d
CK-8d vs DBD-8d
B
CK-0d vs DBD-8d
23
25
8
15
321
579
163
CK-0d vs CK-8d
CK-8d vs DBD-8d
F
CK-0d vs CK-8d
Protein number
Cupin
Late embryogenesis abundant protein
Oleosin
14-3-3 protein
Papain family cysteine protease
AMP-binding enzyme
Glutathione S-transferase, N-terminal domain
Cytochrome P450
RNA recognition motif
UDP-glucoronosyl and UDP-glucosyl transferase
C
COG Function Classification of Consensus Sequence
CK-0d vs CK-8d
Translation, ribosomal structure and biogenesis
RNA processing and modification
Transcription
Replication, recombination and repair
Chromatin structure and dynamics
Cell cycle control, cell division, chromosome partitioning
Nuclear structure
Defense mechanisms
Signal transduction mechanisms
Cell wall/membrane/envelope biogenesis
Cell motility
Cytoskeleton
Extracellular structures
Intracellular trafficking, secretion, and vesicular transport
Posttranslational modification, protein turnover, chaperones
Energy production and conversion
Carbohydrate transport and metabolism
Amino acid transport and metabolism
Nucleotide transport and metabolism
Coenzyme transport and metabolism
Lipid transport and metabolism
Inorganic ion transport and metabolism
Secondary metabolites biosynthesis, transport and catabolism
General function prediction only
Function unknown
Mobilome: prophages, transposons
Frequency
G
CK-0d vs DBD-8d
Protein number
Cupin
Late embryogenesis abundant protein
AMP-binding enzyme
Cytochrome P450
Oleosin
RNA recognition motif
14-3-3 protein
Cellulose synthase
Glutathione S-transferase, N-terminal domain
UDP-glucoronosyl and UDP-glucosyl transferase
D
COG Function Classification of Consensus Sequence
CK-0d vs DBD-8d
Frequency
E
COG Function Classification of Consensus Sequence
CK-8d vs DBD-8d
Frequency
H
CK-8d vs DBD-8d
Protein number
ASCH domain
Acetamidase/Formamidase family
Acetyltransferase (GNAT)family
C-terminus of histone H2A
RNA recognition motif
TB2/DP 1, HVA22 family
linker histone H1 and H5 family
Aromatic amino acid lyase
Hsp20/alpha crystallin family
Probable lipid transfer

1127

Fig. 6. Quantitative proteomic analysis of sweet corn. Number statistics of differentially expressed proteins (DEPs) in three comparisons (A), Venn diagram of DEPs across three comparative groups (B), COG functional classification of DEPs in CK-0d vs CK-8d (C), COG functional classification of DEPs in CK-0d vs DBD-8d (D), COG functional classification of DEPs in CK-8d vs DBD-8d (E), the top 10 most abundant Pfam domain family counts of DEPs in CK-0d vs CK-8d (F), the top 10 most abundant Pfam domain family counts of DEPs in CK-0d vs DBD-8d (G), the top 10 most abundant Pfam domain family counts of DEPs in CK-8d vs DBD-8d (H) for CK and DBD-treated sweet corn.

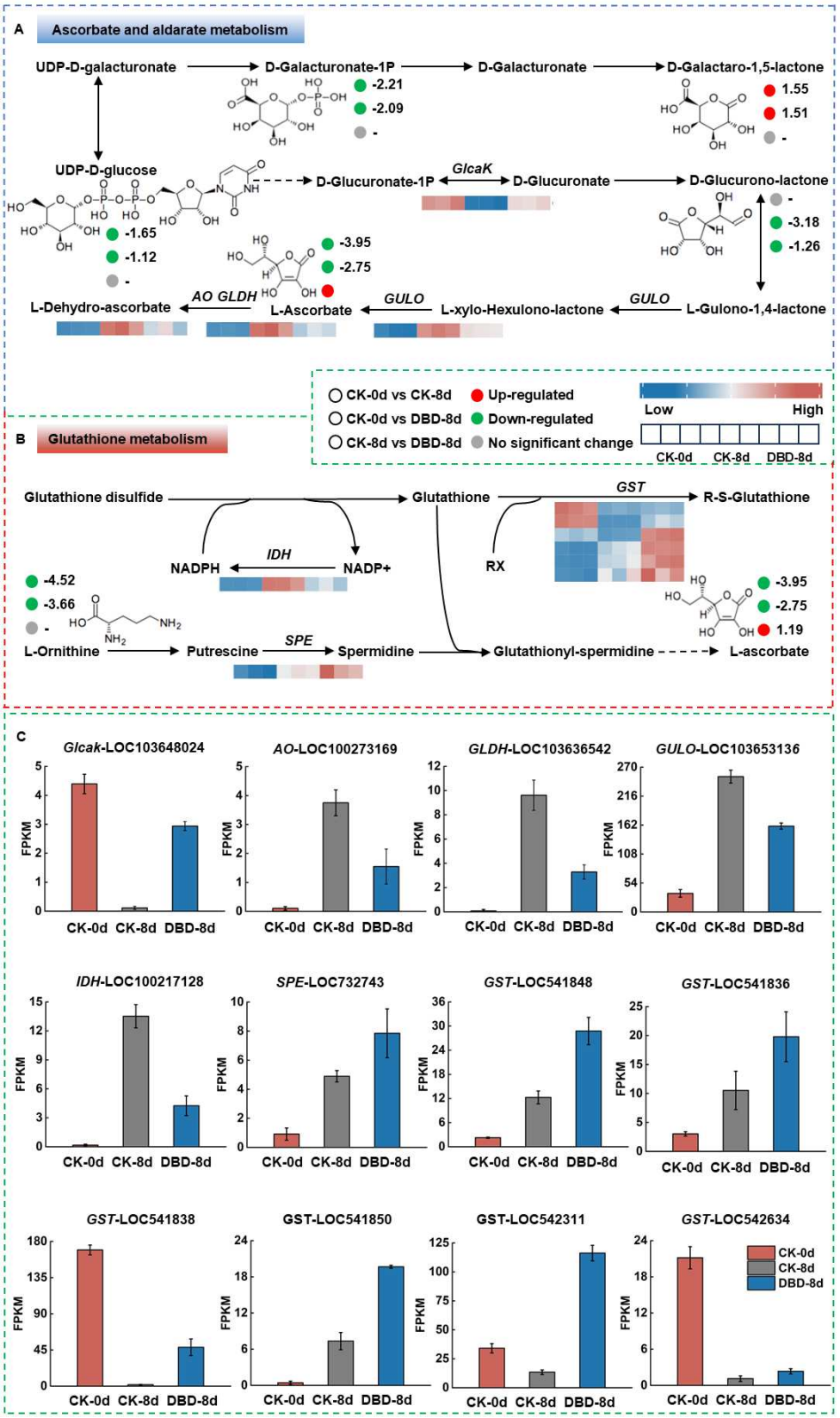
A
Ascorbate and aldarate metabolism
UDP-D-galacturonate
D-Galacturonate-1P
D-Galacturonate
D-Galactaro-1,5-lactone
-2.21
-2.09
1.55
1.51
UDP-D-glucose
D-Glucuronate-1P
GlcaK
D-Glucuronate
D-Glucurono-lactone
-1.65
-1.12
-3.95
-2.75
-3.18
-1.26
L-Dehydro-ascorbate
AO GLDH
L-Ascorbate
GULO
L-xylo-Hexulono-lactone
GULO
L-Gulono-1,4-lactone
CK-0d vs CK-8d
CK-0d vs DBD-8d
CK-8d vs DBD-8d
Up-regulated
Down-regulated
No significant change
Low
High
CK-0d
CK-8d
DBD-8d
B
Glutathione metabolism
Glutathione disulfide
Glutathione
GST
R-S-Glutathione
NADPH
IDH
NADP+
RX
-4.52
-3.66
-3.95
-2.75
1.19
L-Ornithine
Putrescine
SPE
Spermidine
Glutathionyl-spermidine
L-ascorbate
C
Glcak-LOC103648024
AO-LOC100273169
GLDH-LOC103636542
GULO-LOC103653136
IDH-LOC100217128
SPE-LOC732743
GST-LOC541848
GST-LOC541836
GST-LOC541838
GST-LOC541850
GST-LOC542311
GST-LOC542634
FPKM
CK-0d
CK-8d
DBD-8d

Fig. 7. Multi-omics integrated visualization of AsA-GSH pathway modulated by DBD plasma. This KEGG pathway diagram displays gene heatmaps based on FPKM values after row-wise Z-score transformation. Changes of key genes and metabolites in ascorbate and aldarate metabolism pathway (A), multi-omics regulatory patterns of core genes in glutathione metabolism pathway (B) for CK and DBD-treated sweet corn. Error bars represent the standard error of the mean of three biological replicates.

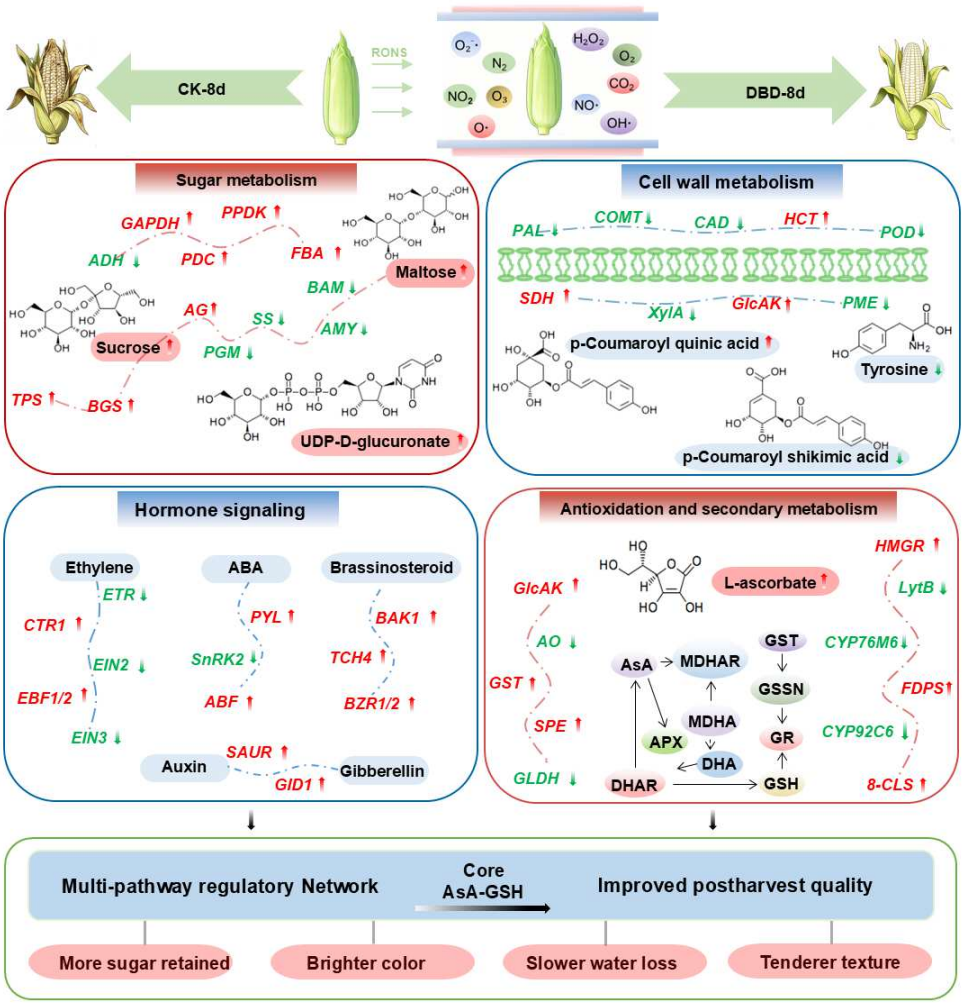

Fig. 8. Proposed working molecular model illustrating how DBD-generated RONS trigger the AsA-GSH-centered multi-pathway synergistic network to delay postharvest senescence of sweet corn. Exogenous RONS derived from DBD plasma act as moderate oxidative signals to activate the AsA-GSH antioxidant network, which further coordinately modulates hormone signal transduction, sugar metabolism, cell-wall metabolism and secondary metabolism, and finally alleviates postharvest quality deterioration of sweet corn. In this schematic diagram, red upward arrows beside genes or metabolites indicate up-regulation, and green downward arrows indicate down-regulation in the comparison of CK-8d vs DBD-8d.

Supplementary Files

This is a list of supplementary files associated with this preprint. Click to download.

- FigureS1.png
- FigureS2.png
- FigureS3.png
- TableS1.xlsx
- TableS2.xlsx
- TableS3.xlsx
- TableS4.xlsx
- TableS5.xlsx
- TableS6.xlsx